iScience

CellPress

Article

Biased Signaling of the Mu Opioid Receptor Revealed in Native Neurons

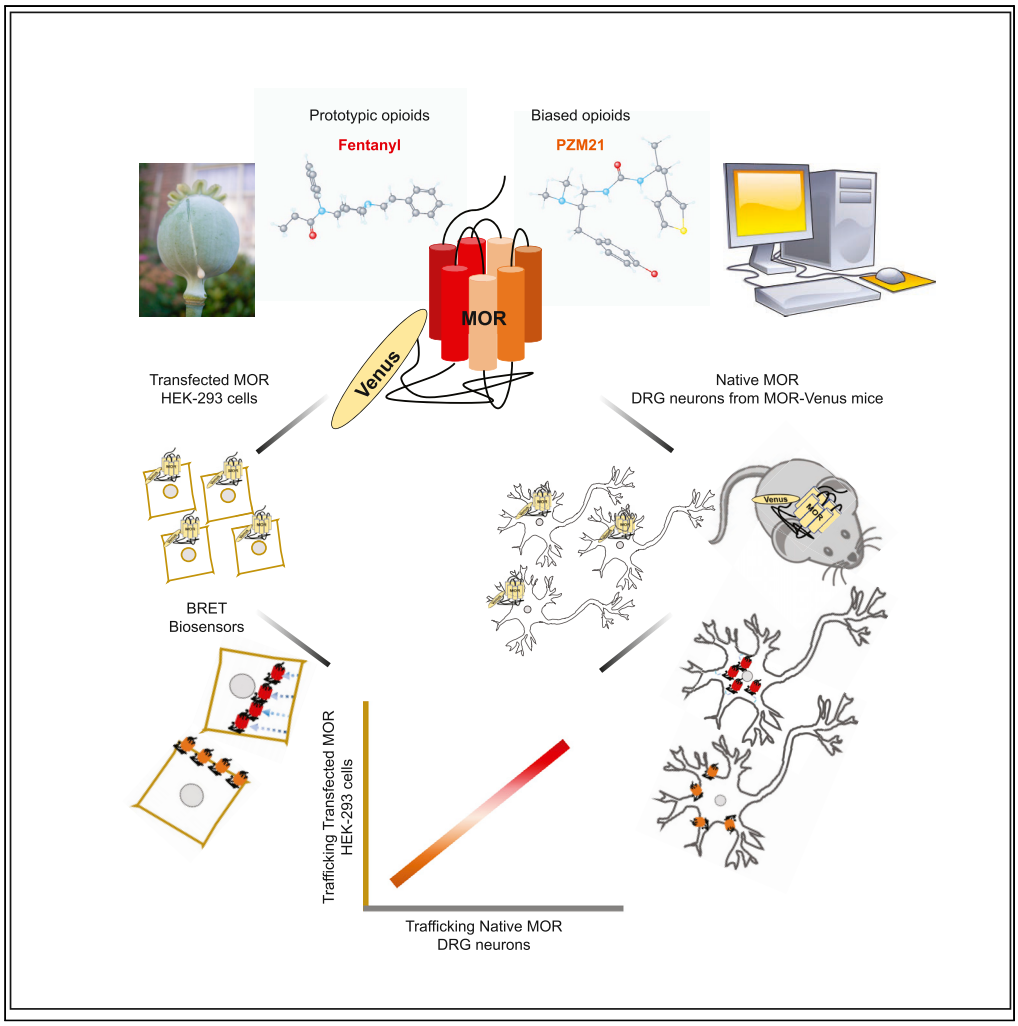

Aliza T. Ehrlich, Meriem Semache, Florence Gross, ..., Emmanuel Darcq, Michel Bouvier, Brigitte L. Kieffer

michel.bouvier@umontreal.ca (M.B.)
brigitte.kieffer@douglas.mcgill.ca (B.L.K.)

HIGHLIGHTS

BRET sensors profiled MOR signaling and trafficking responses in HEK293 cells

MOR-Venus knock-in mice were created to monitor MOR trafficking in DRG neurons

MOR trafficking responses to opioids were correlated between HEK cells and neurons

Of the 10 opioid drugs tested, most remarkable were TRV130, PZM21, and buprenorphine

Ehrlich et al., iScience *14*, 47–57
April 26, 2019
https://doi.org/10.1016/j.isci.2019.03.011

iScience

CellPress

Article

Biased Signaling of the Mu Opioid Receptor Revealed in Native Neurons

Aliza T. Ehrlich,[1,3,5] Meriem Semache,[2,5] Florence Gross,[1,2] Dillon F. Da Fonte,[1] Leonie Runtz,[1] Christine Colley,[1,4] Amina Mezni,[1,4] Christian Le Gouill,[2] Viktoriya Lukasheva,[2] Mireille Hogue,[2] Emmanuel Darcq,[1] Michel Bouvier,[2,*] and Brigitte L. Kieffer[1,3,6,*]

SUMMARY

G protein-coupled receptors are key signaling molecules and major targets for pharmaceuticals. The concept of ligand-dependent biased signaling raises the possibility of developing drugs with improved efficacy and safety profiles, yet translating this concept to native tissues remains a major challenge. Whether drug activity profiling in recombinant cell-based assays, traditionally used for drug discovery, has any relevance to physiology is unknown. Here we focused on the mu opioid receptor, the unrivalled target for pain treatment and also the key driver for the current opioid crisis. We selected a set of clinical and novel mu agonists, and profiled their activities in transfected cell assays using advanced biosensors and in native neurons from knock-in mice expressing traceable receptors endogenously. Our data identify Gi-biased agonists, including buprenorphine, and further show highly correlated drug activities in the two otherwise very distinct experimental systems, supporting *in vivo* translatability of biased signaling for mu opioid drugs.

INTRODUCTION

G protein-coupled receptors (GPCRs) play central roles in cell communication and physiology. These receptors form the largest class of proteins considered for drug discovery and are the targets for about 30% of pharmaceuticals in current use (Wacker et al., 2017). A key advance in GPCR research was the recognition that these receptors are highly dynamic proteins that adopt multiple conformations upon activation by different ligands. As a corollary, distinct agonists acting at the same receptor can engage different effector subsets, modifying cellular outcomes differently and producing distinguishable effects at system level. This concept, termed *biased signaling* or *functional selectivity* (Galandrin et al., 2007; Kenakin, 2011) forms the basis of many high-throughput screening programs to develop novel drugs with improved therapeutic potential (Wacker et al., 2017). At present, biased activities are typically established in engineered heterologous cells, overexpressing receptors and effectors, and the translation to native tissues and living organisms remains a true challenge (Zhou and Bohn, 2014). Although critical for drug development strategies, the extent to which biased signaling in recombinant cells relates to physiology remains largely unknown.

The mu opioid receptor (MOR), a GPCR family member, has emerged as a highly debated drug target as the opioid crisis intensifies in Western countries (Compton et al., 2016). This major public health crisis stems from the overprescription of opioid pain medication, leading to a sharp increase of deaths by overdoses and a devastating shift to heroin (Compton et al., 2016) and fentanyl (Suzuki and El-Haddad, 2017) abuse. However, the pain-relieving efficacy of opioids remains unmatched and, more than ever, developing opioids with low abuse potential and reduced side effects is a major goal in pain research. Among current strategies (Olson et al., 2017) toward safer opioid analgesics (Siuda et al., 2017), the design of biased MOR agonists is considered most promising. Functional selectivity at MOR, with preferential engagement of inhibitory G proteins (Gαi/o) (Gi-biased) or βarrestins (βarr-biased), is well established in heterologous cells (McPherson et al., 2010). In addition, evidence from genetic mouse mutants has suggested that limiting βarr2 recruitment at the receptor would maintain morphine analgesia but reduce adverse effects, including deadly respiratory depression (Zhou and Bohn, 2014). These promising Gαi/o-biased MOR agonists are thus developed using recombinant cell-based assays, leading notably to TRV130 (DeWire et al., 2013) undergoing clinical trials (Singla et al., 2017; Siuda et al., 2017) (and see clinicaltrials.gov), or PZM21, a novel chemotype optimized from *in silico* modeling and docking studies (Manglik et al., 2016). Recently, the extent of Gαi versus βarr bias for MOR ligands was proposed to correlate at the behavioral level with

[1]Department of Psychiatry, McGill University, Douglas Hospital Research Center, Perry Pavilion Room E-3317.1, 6875 Boulevard LaSalle, Montréal, QC H4H 1R3, Canada

[2]Department of Biochemistry and Molecular Medicine, Institute for Research in Immunology and Cancer, Unité de Recherche en Pharmacologie Moléculaire, Université de Montréal, Pavillon Marcelle-Coutu Bureau 1306-3, Montréal, QC H3T 1J4, Canada

[3]Institut de Génétique et de Biologie Moléculaire et Cellulaire, 67400 Illkirch-Graffenstaden, France

[4]Department of Biochemical Sciences, Faculty of Health and Medical Sciences, University of Surrey, Guildford, Surrey GU2 7XH, UK

[5]These authors contributed equally

[6]Lead Contact

*Correspondence: michel.bouvier@umontreal.ca (M.B.), brigitte.kieffer@douglas.mcgill.ca (B.L.K.)

https://doi.org/10.1016/j.isci.2019.03.011

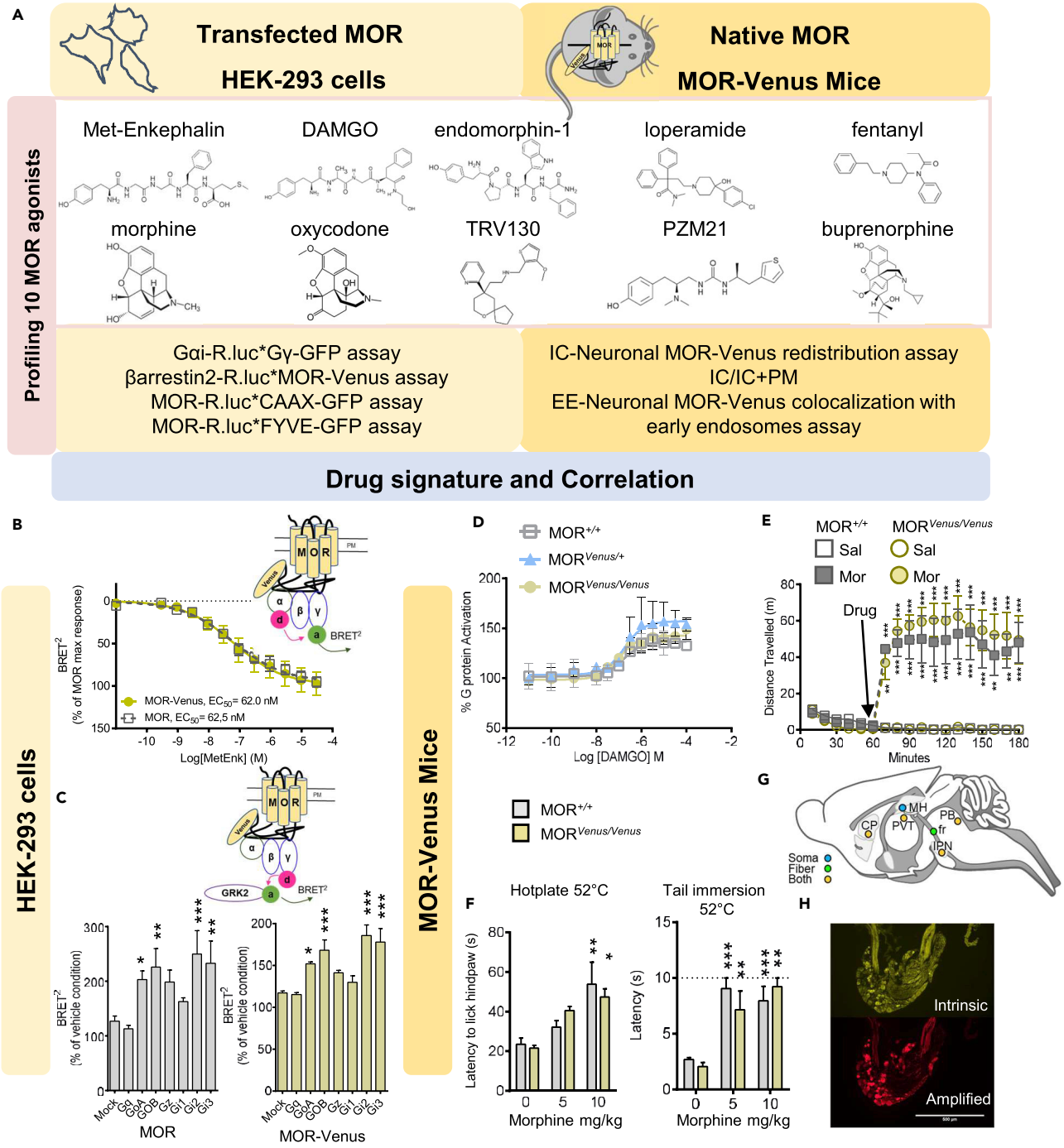

Figure 1. Experimental Strategy and Receptor/Effector Tools

(A) Overview of the two experimental systems (left, transfected biosensors in HEK293 cells; right, knock-in mice expressing MOR-Venus at endogenous levels in place of the native receptor), structure of the 10 MOR agonists tested in the study, assays developed for each experimental system.

(B–H) Functional characterization of MOR-Venus in HEK293 cells (B and C) and *in vivo* (D–H). (B) On top, schematic representation of the Gαi1/Gγ2-BRET^2 biosensor assay. Upon ligand binding to the receptor, Gαi1-RlucII (d, donor) dissociates from the βγ-GFP10 (a, acceptor) dimer, which results in a decrease in BRET^2 signal. Data are expressed as % of BRET signal for MOR (untagged), four replicate experiments. (C) G protein activation profile for MOR and MOR-Venus. On top, schematic representation of the pan Gγ/GRK-based BRET^2 assay, Gγ3-RlucII (d, donor), and GRK2-GFP10 (a, acceptor). Upon ligand binding to the receptor, the Gα subunit dissociates from the βγ-RlucII dimer allowing recruitment of GRK2-GFP10 increasing the BRET^2 signal. BRET^2 was measured 10 min after stimulation with 30 μM Met-Enk. Mock shows MOR-mediated activation of endogenous G proteins. Data are expressed as percentage mock response (n = 3–5 independent experiments, one-way ANOVA). (D) There was no difference in G protein signaling in the striatum of MOR and MOR-Venus

Figure 1. *Continued*

mice. [S^{35}] GTPγS incorporation in striatal membranes prepared from $MOR^{+/+}$(wild-type controls), $MOR^{Venus/+}$ (heterozygous knock-in), and $MOR^{Venus/Venus}$ (homozygous knock-in) mouse littermates, in response to increasing DAMGO concentrations. Data are expressed as mean % activation ± SEM of [S^{35}] GTPγS binding above basal (no agonist) level (3–4 independent experiments with duplicates). Two-way ANOVA found no difference of drug effects across genotypes. (E) $MOR^{+/+}$ and $MOR^{Venus/Venus}$ injected with morphine (40 mg/kg i. p.) or saline show similar locomotor responses (10-min bins). Data are expressed as the distance traveled in centimeters (n = 5–6/group, two-way ANOVA, significant drug effect, no genotype effect). (F) Morphine analgesia is intact in MOR and MOR-Venus mice. Animals were injected with morphine (5 or 10 mg/kg intraperitoneally) or saline. Left, analgesia in the hot plate test, measured by latency to lick the hind paw (n = 3–4/group, two-way ANOVA, significant drug effect at 10 mg/kg, no genotype effect). Right, analgesia in the tail immersion test (52°C), measured by tail withdrawal latency (n = 3–4/group, two-way ANOVA, significant drug effect at 5 and 10 mg/kg, no genotype effect). Cutoff to be removed from the test (10 s) is indicated by a broken line. (G) Whole-brain mapping of MOR-Venus expression (quantification in Table S1). The scheme shows an overview of MOR-Venus distribution in soma (blue), fibers (green), or both (gold) across brain areas enriched for the receptor. MH, medial habenula; fr, fasciculus retroflexus; IPN, interpeduncular nucleus; CP, caudate putamen; PVT, paraventricular thalamus; PB, parabrachial nucleus. (H) Sections of MOR-Venus dorsal root ganglia (DRG) detect MOR either directly (intrinsic, Venus fluorescence) or using Venus amplification (anti-Venus antibody, amplified). All data in (B–F) are presented as mean ± SEM. Statistical significance is defined as *p < 0.05, **p < 0.01, ***p < 0.001.

the analgesia or respiratory depression therapeutic window (Schmid et al., 2017). Until now, however, evidence for the direct translation of biased signaling observed in engineered cells to living neurons is lacking. In this study, we designed a novel strategy (Figure 1A) to address this key point, and our data provide the long-awaited demonstration that biased signaling properties of both traditional and newly developed MOR agonists operate similarly in native neurons.

RESULTS

Designing the MOR-Venus Tool in Recombinant Cells

We first designed a customized version of MOR amenable to distinguish agonist activities in a physiological context. As agonist-induced MOR trafficking is considered a hallmark of biased signaling (Williams et al., 2013), and is a measurable endpoint *in vivo*, we created an MOR version that would be traceable in tissues. Guided by our previous work (Erbs et al., 2015), we fused the mouse MOR to Venus-YFP (MOR-Venus) the most versatile fluorophore compatible with resonance energy transfer (RET) biosensors (Breton et al., 2010) and best detectable in living cells (Nagai et al., 2002). We tested the integrity of MOR-Venus signaling in HEK293 cells, typically used for drug screening and signaling assays. In a Gαi/Gγ-dissociation bioluminescence RET^2 (BRET) biosensor assay (Gales et al., 2006), the reference MOR endogenous opioid Met-enkephalin (Met-Enk) stimulated Gαi1 with similar potency and efficacy in recombinant MOR (untagged) and MOR-Venus (tagged) receptors (Figure 1B). In a pan G protein Gγ/GPCR kinases (GRKs) recruitment-based $BRET^2$ assay (Karamitri et al., 2018), absolute values for basal G protein signaling were comparable between untagged and tagged receptors (Figure S1A). Furthermore, Met-Enk promoted activation of all Gαi and Gαo family members, but was inactive at Gαq for both MOR and MOR-Venus (Figure 1C). Also, similar preference toward GαoA, GαoB, Gαi2, and Gαi3 was found for the two receptors. Finally, we created a human version of MOR-Venus, and tested both mouse and human receptors for the activation of 7 mouse and 14 human Gα subunits, using the Gγ/GRK-based $BRET^2$assay (Figures S1B–S1E). This comprehensive profiling showed no difference in Met-Enk responses, whether the receptor was mouse or human or tagged or untagged, or whether Gα was mouse or human. Altogether, these data suggest that the Venus fusion does not alter receptor signaling and supports data translatability between mouse and human MOR signaling.

Creating the MOR-Venus Mouse to Tackle Physiological Signaling

We then created the corresponding MOR-Venus knock-in mouse line by homologous recombination, so that MOR-Venus is expressed in place of the native receptor (Figure S2A). MOR mRNA levels in brain samples from $Oprm1^{Venus/Venus}$ homozygous (MOR-Venus mice), $Oprm1^{Venus/+}$ heterozygous, and $Oprm1^{+/+}$ control littermates were comparable (Figure S2B), and [D-Ala^2, N-$MePhe^4$, Gly-ol]-enkephalin (DAMGO)-induced G protein activation in striatal membranes showed superimposable dose-responses for all three genotypes (Figure 1D). Morphine-induced locomotor stimulation (Figure 1E) and analgesia (Figure 1F) were also intact in MOR-Venus mice, indicating altogether that the MOR-Venus receptor is expressed at levels comparable to endogenous receptors in the animal and is fully functional. MOR-Venus distribution analysis showed co-localized expression of both tagged and untagged receptors in heterozygous animals (Figure S3). Mapping throughout the nervous system revealed an MOR-Venus expression pattern consistent with previous reports (Figures S4A–S4C, Table S1, and see Erbs et al., 2015) and provided additional details on MOR localization in soma or fibers (Figure 1G). Finally, MOR-Venus expression in sensory neurons

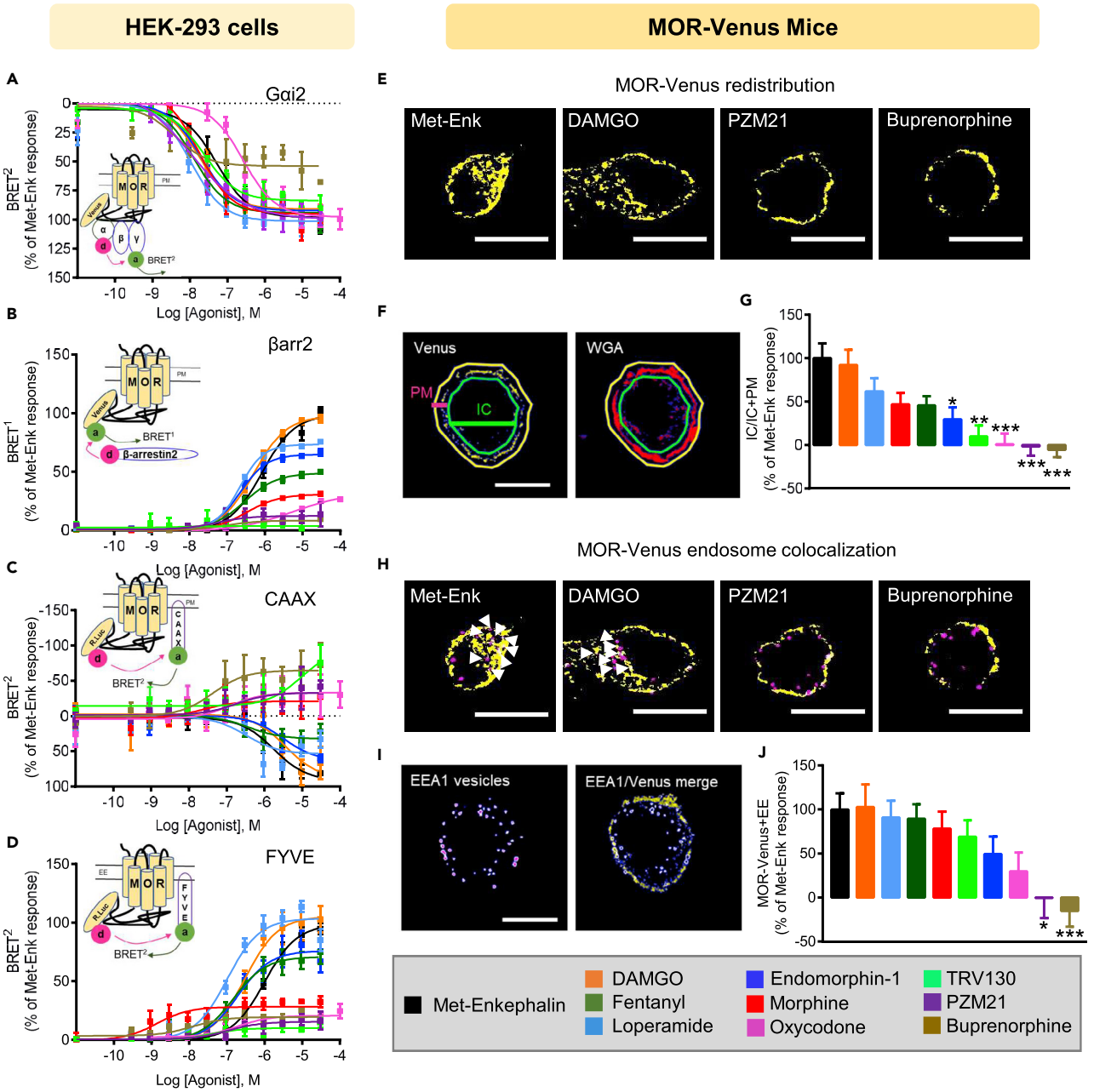

Figure 2. Profiling MOR Agonists in the Two Experimental Systems

(A–J) Data obtained from HEK293 cells overexpressing MOR-Venus (A–D) and DRG neurons from MOR-Venus mice (E–J). (A) Gαi2 responses in HEK293 cells. On top, schematic representation of the Gαi2/Gγ2-BRET^2 biosensor assay with BRET^2 sensors (Gαi2-RlucII, d, donor; Gγ2-GFP10, a, acceptor). Cells were stimulated 10 min with increasing concentrations of the indicated compound. Data are expressed as % of Met-Enk response n = 3–7 independent experiments. (B) βarr2 recruitment in HEK293 cells. On top, schematic representation of the MOR/βarr2 BRET^1 biosensor assay. Upon activation, RlucII-tagged βarr2 (d, donor) is recruited to MOR-Venus (a, acceptor), resulting in increased BRET^{1}signal. Cells were stimulated 10 min with increasing concentrations of the indicated compound. Data are expressed as mean % of the maximal response induced by Met-Enk (n = 4–9 independent experiments). (C) Receptor internalization in HEK293 cells. On top, schematic representation of the MOR/CAAX BRET^2 biosensor assay, used to monitor receptor disappearance from the plasma membrane (PM). MOR-RlucII is the donor (d), and rGFP-tagged CAAX is the acceptor (a). HEK293 cells were exposed to increasing concentrations of MOR agonists for 30 min. Data are expressed as % of Met-Enk response (4–7 independent experiments). (D) Receptor translocation to endosomes in HEK293 cells. On top, schematic representation of MOR/FYVE BRET^2 biosensor assay, used to monitor receptor translocation to early endosomes (EE). MOR-RlucII is the donor (d), and rGFP-tagged FYVE is the acceptor (a). HEK293 cells were exposed to increasing concentrations of MOR agonists for 30 min. Data are expressed as mean % of the maximal response induced by Met-Enk (n = 4–7 independent experiments). (E–G) Receptor redistribution in DRG neurons. (E) DRG neurons from adult MOR-Venus mice were dissociated and exposed to 1 μM MOR agonist for 10 min. Representative

Figure 2. *Continued*

confocal images are shown after thresholding (see Transparent Methods) and reveal MOR-Venus redistribution to intracellular compartments for Met-Enk and DAMGO (left panel) but not PZM21 and buprenorphine (two right panels). Scale bar, 10 μm. (F) Quantification method. A vehicle-treated neuron illustrates the method used to quantify MOR-Venus redistribution in neurons (anti-Venus antibody; left, yellow, plasma membrane (PM) label; WGA-Alexa594, right, red). PM and intracellular (IC) compartments were defined by drawing regions of interest (PM, yellow outer line; IC, green inner line). Fluorescence intensity was measured in the two compartments, quantified as IC/total (IC + PM), and vehicle was subtracted. (G) MOR-Venus redistribution following treatment with the 10 MOR compounds. Data are expressed as %IC/IC + PM of the Met-Enk response (n = 26–52 cells per drug condition). (H–J) Receptor co-localization to early endosomes (EEs) in DRG neurons. (H) Representative confocal images show MOR-Venus DRG neurons exposed to 1 μM MOR agonist for 10 min and immunostained to amplify MOR-Venus (anti-Venus antibody, yellow) and label EEs (anti-EEA1 antibody, magenta). Met-Enk and DAMGO (left panel), but not PZM21 and buprenorphine (2 right panels), increases MOR-Venus/EE co-localization. Scale bar, 10 μm; white arrowheads locate double-positive MOR-Venus/EEA1 vesicles. (I) Quantification method. A vehicle-treated cell illustrates the method of quantification in the EE assay. Confocal images were thresholded (see Transparent Methods), and individual vesicles were outlined as ROI using the EEA1 channel. ROI were then counted in either EEA1 or Venus channels to determine the number of EEA1 vesicles containing MOR-Venus. (J) MOR-Venus co-localization with EEs following treatment with the 10 MOR compounds. Data are expressed as % of Met-Enk response (n = 26–42 cells per drug condition). All data in (A–D), (G), and (J) are shown as mean ± SEM. Statistical significance of the differences (G and J, one-way ANOVA) is defined as *$p < 0.05$, **$p < 0.01$, ***$p < 0.001$ versus Met-Enk condition.

of dorsal root ganglia (DRGs, see Figure 1H) matched the known predominant MOR expression in first-order nociceptive neurons (Scherrer et al., 2009). MOR-Venus mice, therefore, provide an ideal physiological assay system to profile MOR agonist activities, under conditions that recapitulate native receptor expression.

Profiling Drug Activities for 10 Mu Opioid Agonists in Recombinant Cells

Next, we measured the activities of selected opioid agonists at MOR-Venus, in the HEK293 cell heterologous system. The 10 selected compounds included prescribed or abused MOR agonists (morphine, oxycodone, buprenorphine, fentanyl), prototypic peptidic compounds (Met-Enk, DAMGO, endomorphin-1), and Gαi/o-biased agonists from recent drug discovery efforts (TRV130, PZM21) (Figure 1A).

In HEK293 cells, concentration-response curves for Gαi2 activation using Gαi/Gγ-BRET^2 showed highly similar curves for all the drugs, except for oxycodone, which had a trend of lower potency and for buprenorphine, which had significantly lower efficacy and potency than Met-Enk (Figure 2A and Table S2). Testing all three Gαi subunits in the Gαi/Gγ-BRET^2 biosensor assay revealed no significant difference in basal activity for MOR-Venus and untagged MOR (Figures S5A and S5B), and highly similar drug responses for Gαi1 and Gαi3 (Figures S5C and S5D).

To test βarr2 recruitment, we used the Venus fusion of MOR as the BRET^1 acceptor for βarrestin-RlucII (Figure 2B) and obtained robust BRET responses, indicating that MOR-Venus itself may be used as a biosensor. We obtained a wide range of responses for the 10 drugs, suggesting that βarr2 engagement is a better differentiating factor than the Gαi response. Co-expressing GRKs 2, 5, or 6 increased βarr2 recruitment for most drugs (Figure S6B) as expected (Ribas et al., 2007; Williams et al., 2013), although notably the effect was modest for TRV130, PZM-21, and buprenorphine (Tables S3A and S3B). Of note, the Venus tag did not modify basal βarr2 recruitment, as there was no significant difference between MOR-Venus and untagged MOR in a control experiment measuring basal βarr2 recruitment (Figure S6A).

We next used our recently developed enhanced bystander (ebBRET) biosensors (Figures S7A and S7D) to monitor receptor redistribution upon agonist exposure (Namkung et al., 2016), an event tightly linked to βarr2 engagement. In receptor-independent control experiments, we found that untagged MOR and MOR-Venus showed no statistical difference in their activities to translocate βarr2 to endosomes, either in the absence of agonist (Figure S7B) or in the presence of Met-Enk (Figure S7C). As the MOR tag had no apparent effect in this assay, we next compared the 10 selected compounds using MOR-RlucII as the donor to directly monitor receptor redistribution upon agonist exposure (Figure S7D). As expected, Met-Enk promoted receptor disappeared from the plasma membrane (PM), detected using the rGFP-CAAX biosensor, and the receptor concomitantly accumulated in early endosomes (EE), detected using rGFP-FYVE (Figures S7D and S7E). As for βarr2 profiling, testing the 10 drugs showed a wide range of activities in both CAAX (Figure 2C) and FYVE (Figure 2D) assays. The observation that buprenorphine, and to a lesser extent oxycodone and morphine, increased the CAAX BRET signal (Table S4) suggests that these drugs may, in fact, inhibit constitutive endocytosis or recruit more receptors to the PM. In the FYVE assay, agonists induced receptor translocation to endosomes to a similar extent for all compounds except morphine, oxycodone, PZM21, TRV130, and buprenorphine, which had significantly lower efficacies

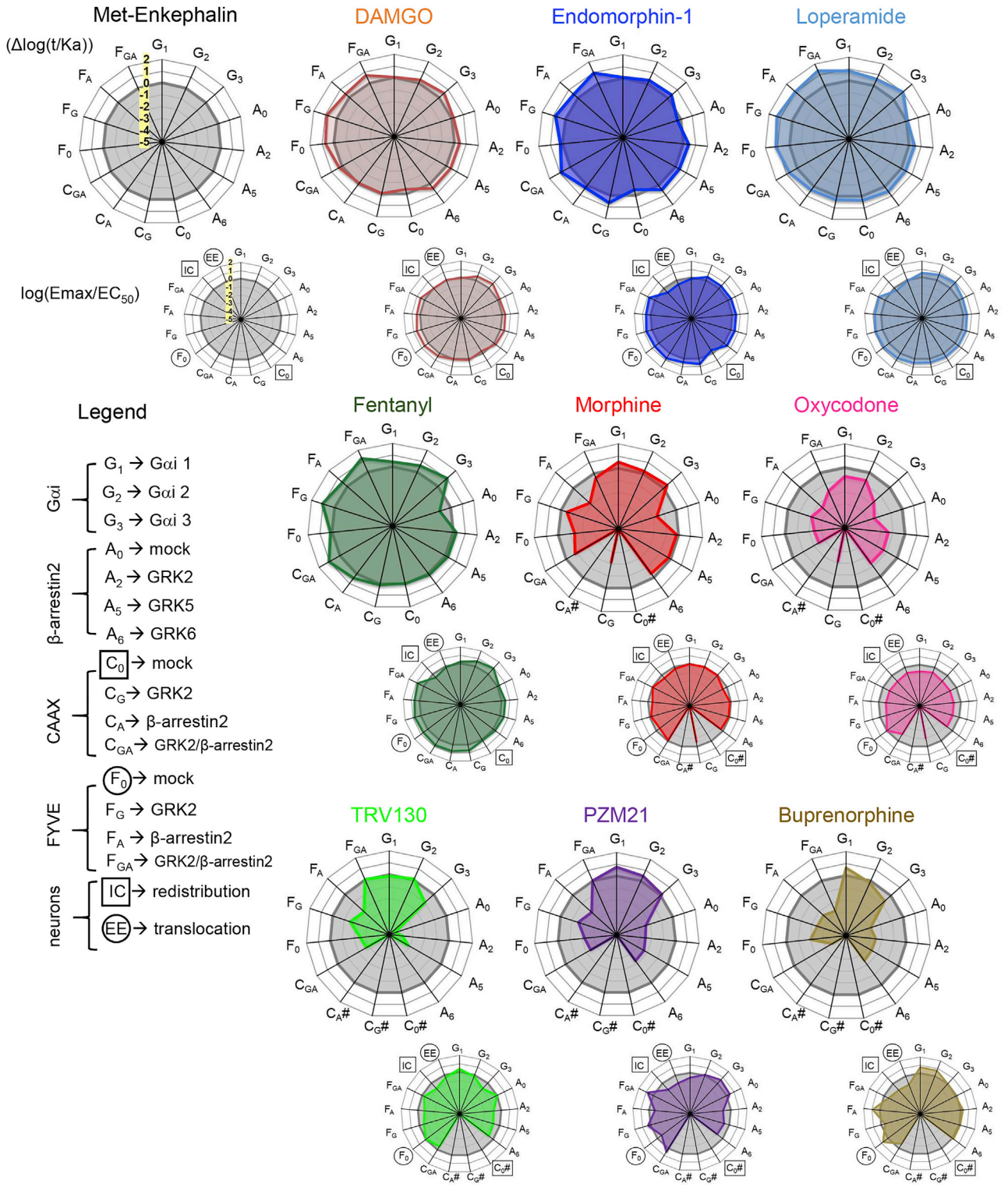

Figure 3. Buprenorphine Stands Out among 10 Signatures of MOR Agonists

Radial graphs illustrating the specific activity signature (see Transparent Methods) for each drug (colored line) compared with Met-Enk (gray line). Upper radial plots: dose-response curves for the HEK293 cell data were used to derive the logarithm of the "transduction coefficients" (Δlog(τ/Ka)) to integrate efficacy (τ) and affinity (Ka). Lower radial plots integrate single concentration effect in neurons and dose-response effects in HEK293 cell data as follows: dose-response curves were used to fit HEK293 cell data into an Emax/EC_{50} ratio to estimate signaling efficacy, whereas the neuronal (DRG) data (Figure 2G or

Figure 3. *Continued*

2J), where all drug treatments were done at submaximal dose (Figure S8B), were normalized as ((compound/Met-Enkephalin)-Met-Enkephalin), thus Met-Enkephalin response is set to 0. For both HEK293 cells and native neurons positive and negative values denote a better or a lower response when compared with Met-Enkephalin. Top left, the scale is highlighted in yellow on the reference Met-Enk radial plot (min −5 to max 2 with intervals of 1). The legend indicates the assay abbreviations. # Indicates a drug effect that was too low or could not be fitted to the operational model.

when compared with Met-Enk (Figure 2D and Table S5). Overexpression of GRK2 alone or in the presence of βarr2 (Figures S7F and S7G) enhanced both the loss of receptor from the PM (CAAX) and their translocation to EE (FYVE) for most drugs (Tables S4 and S5). Exceptions were PZM21, TRV130, and buprenorphine with significantly lower efficacies in the CAAX assay when compared with Met-Enk in the presence of GRK2 and βarr2 (Figure S7F and Table S4), and, remarkably, buprenorphine maintained a significantly lower efficacy in the trafficking assay (Figure S7G and Table S5), whereas TRV130 and PZM21 responded to a similar efficacy as Met-Enk.

Profiling Drug Activities for 10 Mu Opioid Agonists in Native Neurons

We then tested the activities of the 10 drugs on DRG neurons, which we extracted from adult MOR-Venus mice. These cells are most relevant to pain control and well suited for quantification by confocal imaging (Figure S8A). PM was labeled using WGA-AlexaFluor594, and fluorescence in intracellular (IC) compartment versus PM was compared (Figure 2F thereafter called IC assay). DAMGO dose- and time-dependently increased the translocation of MOR-Venus signal intracellularly (Figure S8B), indicating the sub-maximal dose as 1 μM and 10-min time point for the best assay conditions to compare the 10 drugs for their ability to promote endocytosis in neurons. MOR-Venus DRG neurons were then exposed to each drug and imaged (Figures 2E–2G, S9A, and S9B). A range of effects was obtained, from compounds producing MOR-Venus redistribution similar to Met-Enk-induced responses (DAMGO) to those that significantly differed either only weakly redistributing (TRV130, oxycodone), or even increasing MOR-Venus at the PM (PZM21 and buprenorphine) (Figures 2G and S9A and Table S6). Furthermore, agonist-induced receptor redistribution was not modified by the level of MOR-Venus expression, as high- and low-MOR-Venus-expressing neurons showed similar responses (Figure S10A) and Pearson correlation between IC assay and total MOR-Venus signals was not significantly correlated ($r = 0.3069$, $p = 0.3883$) for the selected 10 compounds (Figure S10B).

We designed another assay to measure MOR-Venus co-localization to EEs (Figures 2H–2J and S11A–S11C) by overlaying EEA1-positive vesicles in DRG neurons with MOR-Venus fluorescence, and counting for double-positive signals. Overall, drug treatment did not significantly modify the average number of EEA1-labeled vesicles per cell when compared with Met-Enk (Figure S11C) but increased the percentage of vesicles showing EEA1 and MOR-Venus co-localization (Figure 2J). Again, drug effects were compared to Met-Enk responses (Table S7) and ranged from similar (DAMGO) receptor to endosome translocation to none (PZM21), or even opposing (buprenorphine) effect (Figure 2J), consistent with the data obtained with the IC assay.

Establishing Drug Signatures

Altogether the 10 drugs showed a wide range of activities. We next further estimated drug signaling efficacy using the operational model integrating logarithms of the transduction coefficient ($\Delta\log(\tau/Ka)$) derived from concentration-response curves (Black and Leff, 1983) obtained in HEK293 cells (see Methods and Figure 3, upper radial plots). These transduction coefficients were further used to estimate the bias between either Gαi2 and βarr2 or MOR localization to EE compartments (FYVE assay) (Table S8). Notably, this analysis found morphine, oxycodone, TRV130, PZM21, and buprenorphine to be Gαi2-biased for both estimates of bias. Fentanyl showed bias toward Gαi2 over βarr2 in the absence of additional GRK2; however, when GRK2 was added, βarr2 recruitment (Table S3B) was increased to a similar efficacy level as Met-Enk response suggesting that this Gαi2 bias may be dependent on GRK2 availability.

To better illustrate the data, we integrated the overall efficiency of the drugs using the $Emax/EC_{50}$ ratios in HEK293 cells with the 1 μM drug responses in native neurons for each drug in radial graphs (see Methods and Figure 3, lower radial plots), providing a set of MOR agonist signatures. Note that only the HEK293 cell data were derived from concentration-effect values. Agonist profiles formed a continuum, but can essentially be discussed as three groups. DAMGO, endomorphin-1, loperamide, and fentanyl were close to the reference Met-Enk, showing both efficient Gαi and βarr2 activities in HEK293 cells, consistent with previous

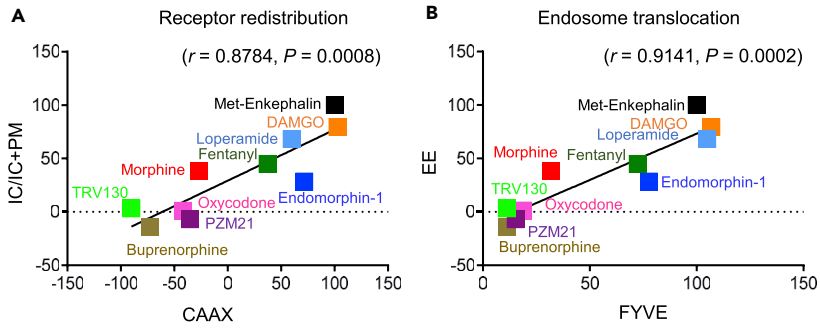

Figure 4. MOR Trafficking Is a Suitable Readout for Ligand-Dependent Activities

Pearson correlation analysis was used to examine the compatibility of trafficking responses for the 10 MOR compounds in two distinct systems. The best comparable assays between transfected MOR-Venus and native MOR-Venus systems were CAAX or FYVE biosensors in HEK293 cells with receptor redistribution to intracellular (IC) or early endosome (EE) compartment assays in DRG neurons. Dose-response curves (Figures 2C and 2D) were used to derive E_{max} values in % of Met-Enkephalin (Met-Enk) from HEK293 cells, and sub-maximal dose neuronal data in % of Met-Enk (Figures 2G and 2J) were used for correlation.

(A) Positive correlation between receptor redistribution in DRG neurons (IC + IC/PM) and HEK293 cell (MOR-Rluc/rGFP-CAAX) assays (Pearson correlation: $r = 0.8784$, $p = 0.0008$).

(B) Between-receptor co-localization with EEs in DRG neurons (EE) and HEK293 cell (MOR-Rluc/FYVE-rGFP) assays (Pearson correlation: $r = 0.9141$, $p = 0.0002$).

studies (Pradhan et al., 2012). Moreover, the four drugs also showed comparable trafficking effects in HEK293 cells (enhanced by GRK2/βarr2 overexpression) and DRG neurons. The second and third groups had in common lower effects in the CAAX assay that made them unable to be fitted to the operational model. In the second group, morphine and oxycodone shared a similar Gαi-biased profile, although oxycodone was less active overall. Morphine in HEK293 cells showed efficient Gαi signaling, whereas βarr2 engagement was marginally observed unless GRKs were overexpressed. Morphine was also able to induce receptor redistribution in HEK293 cells (FYVE and CAAX with GRK2/βarr2 overexpression) as well as under physiological conditions (both IC and EE assays). The third group includes TRV130, PZM21, and buprenorphine; all were Gαi2 biased, but only buprenorphine showed insensitivity to GRK2/βarr2 overexpression in the CAAX and FYVE assays in HEK293 cells. In neurons, subtle differences further distinguished the three compounds. TRV130 moderately increased endosomal co-localization (Figure 2J), whereas PZM21 and buprenorphine did not, possibly due to MOR-Venus externalization (Zaki et al., 2000) and/or stabilization at the PM. Finally, although Gαi-biased profiles were anticipated for TRV130 (Siuda et al., 2017) and PZM21 (Manglik et al., 2016), the extreme position of buprenorphine in our neuron-based assays was striking. Similar to the trafficking responses in the neurons, buprenorphine showed the lowest efficacy in HEK293 trafficking assays despite addition of GRK2/βarr2 (Tables S4 and S5) displaying a signaling signature presumably optimal for a better therapeutic safety window (Schmid et al., 2017). This long-standing prescribed drug for opioid addiction treatment (Ayanga et al., 2016), in fact, has been neglected for pain treatment and may be reconsidered (Ehrlich and Darcq, 2019; Khanna and Pillarisetti, 2015).

Correlating Trafficking Activities in Recombinant Cells and DRG Neurons

Finally, we compared activities of the compounds in the two experimental systems, to directly assess the translatability of HEK293 cell responses to neurons. As IC redistribution and EEA1 colocalization in DRG neurons are best comparable with CAAX and FYVE biosensor responses in HEK293 cells, respectively, we used E_{max} from HEK293 cell dose-response curves (Figures 2C and 2D and Tables S4 and S5) and the sub-maximal-dose-derived percentage Met-Enk neuronal responses (Figures 2G and 2J) for correlation analysis. We found strong positive correlation for both dataset comparisons (Figure 4A, $r = 0.8784$ and ***$p = 0.0008$; Figure 4B, $r = 0.9141$ and ***$p = 0.0002$). This result demonstrates that biased signaling of MOR agonists, typically established in traditional drug screening systems, is physiologically relevant to neurons.

DISCUSSION

GPCRs constitute the largest family of protein targets for approved drugs in the United States and European Union (Sriram and Insel, 2018), and emerging strategies to design new GPCR-based therapeutics

take advantage of biased signaling to improve efficacy and safety (Ehrlich et al., 2019; Hauser et al., 2017). At present, drug signaling profiles are established using overexpressed receptors and effectors in non-neuronal cells, which are practical for biosensor-based assays, but the translation to endogenous receptors in living neurons remains a major question as receptor density is lower by several orders of magnitude and effector availability is essentially unknown (Luttrell et al., 2018). Here we used the MOR as a model receptor to approach this question. The alarming context of the current opioid epidemic has led to developing novel Gαi/o-biased MOR agonists (TRV130 and PZM21) to limit adverse opioid effects (DeWire et al., 2013; Manglik et al., 2016; Schmid et al., 2017), which we studied here together with clinically used and abused opiates.

Earlier studies that have examined a large set of MOR agonists' ability to activate G proteins, phosphorylate MOR, recruit βarr2, and internalize the receptor (McPherson et al., 2010) have primarily been performed in transfected HEK293 cells. Here we developed a knock-in mouse line, which produces a detectable version of the receptor (MOR-Venus) in place of the native receptor. In HEK293 cells, basal G protein activation profile, βarr2 recruitment, and trafficking to endosomes were comparable for untagged and MOR-Venus-tagged receptors. In the mouse, MOR-Venus mediated behavioral morphine effects (hyperlocomotion and analgesia) similar to the native receptor. MOR-Venus is therefore fully functional in both overexpression HEK293 cell-based assays and in the mouse, providing an ideal tool to compare drug-induced trafficking under artificial and physiological conditions. We found that, the Gαi/o-biased TRV130, PZM21, and buprenorphine induced virtually no receptor redistribution or endosome translocation, whereas clinical and peptidic ligands showed limited to strong trafficking effects, and, importantly, these activities were remarkably correlated in recombinant and physiological assays. Our study therefore provides a long-awaited validation of early-stage preclinical efforts for MOR drug discovery and also holds promise for GPCR drug discovery in general.

Trafficking analyses provided the best differentiation of drug effects in HEK293 cells, and receptor redistribution at subcellular level may represent a further research path to characterize drug activities. Future analysis of MOR-Venus trafficking in distinct cellular compartments may further differentiate drug activities in native neurons and provide novel and perhaps translatable insights into agonist-dependent MOR signaling *in vivo* (Irannejad et al., 2017). Recently, location-specific MOR activation was monitored using a genetically encoded conformational biosensor, and revealed ligand-dependent signaling at the subcellular level, with opioid alkaloid effects detected at the level of Golgi in both soma and dendrites, whereas opioid peptide signaling remaining confined to the PM and EE (Stoeber et al., 2018). Moving forward, these studies and ours reveal novel facets of drug activities by directly observing receptor redistribution intracellularly, which will further refine drug activity profiles. MOR-Venus mice, which were developed for optimal RET, will be a unique tool to develop next-generation biosensors and characterize biased opioid signaling and trafficking *in vivo*.

Buprenorphine (Subutex), which was long used as a treatment for opioid addiction, appears to be a remarkable drug in both overexpression and native systems of this study. In transfected cells, the overexpression of GRK2 and βarr2, known to enhance agonist-induced trafficking, increased responses for all the compounds, including TRV130 and PZM21, but buprenorphine remained largely insensitive. In native neurons, buprenorphine showed the most significant PM-receptor retaining activity in both redistribution and endosome localization assays. The buprenorphine signature, therefore, is closer to recently developed Gi-biased drugs (TRV 130 and PZM21) than any other drug tested in this study. This observation suggests that this clinically safe and efficient analgesic is worth revisiting for pain management as an alternative to common clinical opioids (fentanyl and morphine) (Ehrlich and Darcq, 2019).

To conclude, moving from neuronal cells to whole-organism responses will address yet another level of complexity, and how findings from this study translate to whole animals remains to be seen. Recent improvements in whole animal imaging, for second messengers (Ca^{2+} miniscopes, cAMP *in vivo* biosensors) will be instrumental to fully profile drug signaling *in vivo* (Girven and Sparta, 2017; Kerr and Nimmerjahn, 2012), and ultimately relate circuit-level understanding of biased signaling (Urs et al., 2016) to the amazingly distinct properties of traditional and innovative MOR agonists at the behavioral level (Schmid et al., 2017).

Limitations of the Study

The resolution of MOR-positive DRG neurons was limited in the present study to neurons detected in our primary culture conditions. Future studies, on intact DRG slices or intravital whole animal imaging should

improve the characterization of MOR ligands across all DRG neuronal subtypes and elucidate key actions of these MOR neuronal subsets in pain.

METHODS

All methods can be found in the accompanying Transparent Methods supplemental file.

SUPPLEMENTAL INFORMATION

Supplemental Information can be found online at https://doi.org/10.1016/j.isci.2019.03.011.

ACKNOWLEDGMENTS

This work was supported by the Consortium Québécois de Découverte de Médicaments and the Region Alsace/Biovalley (M.B. and B.L.K.) and Fonds Européen de Développement Régional (B.L.K.). We thank NIDA Drug Supply Program and Alkermes for providing the drugs. We also thank the Mouse Clinic Institute (Illkirch, France) for generating MOR-Venus mice. We thank Aude Villemain, Karine Lachapelle, and DaWoon Park as well as the staff at the Douglas Neurophenotyping Animal Facility for animal care. We thank the Molecular and Cellular Microscopy Platform of the Douglas Mental Health University Institute for microscope usage. We also thank Monique Lagacé for assistance editing the manuscript. This work was also supported by National Institute of Health (National Institute of Drug Abuse Grant No. 05010 to B.L.K.), the Canadian Institutes of Health Research (Grants # MOP11215 and FDN148431 to M.B.), and the Canada Foundation for Innovation. B.L.K. holds the Canada Research Chair in Neurobiology of Addiction and Mood Disorders. M.B. holds the Canada Research Chair in Signal Transduction and Molecular Pharmacology.

AUTHOR CONTRIBUTIONS

Conceptualization, A.T.E., M.B., and B.L.K.; Methodology, A.T.E., M.S., E.D., M.B., and B.L.K.; Formal Analysis, A.T.E., M.S., D.F.D.F., L.R., and F.G.; Investigation, A.T.E., M.S., F.G., D.F.D.F., L.R., C.C., and A.M.; Resources, C.L.G., M.H., and V.L.; Writing – Original Draft, A.T.E. and M.S.; Writing – Reviewing & Editing, A.T.E., M.S., B.L.K., and M.B.; Supervision, M.B. and B.L.K.; Funding Acquisition, M.B. and B.L.K.

DECLARATION OF INTERESTS

The authors declare no potential conflict of interest. Some of the BRET-based biosensors used in this study are the object of patent protection and were licenced to Domain Therapeutics; all BRET-based biosensors can be obtained for non-commercial use through regular academic material transfer agreements.

Received: September 11, 2018
Revised: March 6, 2019
Accepted: March 11, 2019
Published: April 26, 2019

REFERENCES

Ayanga, D., Shorter, D., and Kosten, T.R. (2016). Update on pharmacotherapy for treatment of opioid use disorder. Expert Opin. Pharmacother. *17*, 2307–2318.

Black, J.W., and Leff, P. (1983). Operational models of pharmacological agonism. Proc. R. Soc. Lond. B Biol. Sci. *220*, 141–162.

Breton, B., Lagace, M., and Bouvier, M. (2010). Combining resonance energy transfer methods reveals a complex between the alpha2A-adrenergic receptor, Galphai1beta1gamma2, and GRK2. FASEB J. *24*, 4733–4743.

Compton, W.M., Jones, C.M., and Baldwin, G.T. (2016). Relationship between nonmedical prescription-opioid use and heroin use. N. Engl. J. Med. *374*, 154–163.

DeWire, S.M., Yamashita, D.S., Rominger, D.H., Liu, G., Cowan, C.L., Graczyk, T.M., Chen, X.T., Pitis, P.M., Gotchev, D., Yuan, C., et al. (2013). A G protein-biased ligand at the mu-opioid receptor is potently analgesic with reduced gastrointestinal and respiratory dysfunction compared with morphine. J. Pharmacol. Exp. Ther. *344*, 708–717.

Ehrlich, A.T., and Darcq, E. (2019). Recommending buprenorphine for pain management. Pain Manag. *9*, 13–16.

Ehrlich, A.T., Kieffer, B.L., and Darcq, E. (2019). Current strategies toward safer mu opioid receptor drugs for pain management. Expert Opin. Ther. Targets. https://doi.org/10.1080/14728222.2019.

Erbs, E., Faget, L., Scherrer, G., Matifas, A., Filliol, D., Vonesch, J.L., Koch, M., Kessler, P., Hentsch, D., Birling, M.C., et al. (2015). A mu-delta opioid receptor brain atlas reveals neuronal co-occurrence in subcortical networks. Brain Struct. Funct. *220*, 677–702.

Galandrin, S., Oligny-Longpre, G., and Bouvier, M. (2007). The evasive nature of drug efficacy: implications for drug discovery. Trends Pharmacol. Sci. *28*, 423–430.

Gales, C., Van Durm, J.J., Schaak, S., Pontier, S., Percherancier, Y., Audet, M., Paris, H., and Bouvier, M. (2006). Probing the activation-promoted structural rearrangements in preassembled receptor-G protein complexes. Nat. Struct. Mol. Biol. *13*, 778–786.

Girven, K.S., and Sparta, D.R. (2017). Probing deep brain circuitry: new advances in in vivo calcium measurement strategies. ACS Chem. Neurosci. *8*, 243–251.

Hauser, A.S., Attwood, M.M., Rask-Andersen, M., Schioth, H.B., and Gloriam, D.E. (2017). Trends in GPCR drug discovery: new agents, targets and indications. Nat. Rev. Drug Discov. *16*, 829–842.

Irannejad, R., Pessino, V., Mika, D., Huang, B., Wedegaertner, P.B., Conti, M., and von Zastrow, M. (2017). Functional selectivity of GPCR-directed drug action through location bias. Nat. Chem. Biol. *13*, 799–806.

Karamitri, A., Plouffe, B., Bonnefond, A., Chen, M., Gallion, J., Guillaume, J.-L., Hegron, A., Boissel, M., Canouil, M., Langenberg, C., et al. (2018). Type 2 diabetes-associated variants of the MT_2 melatonin receptor affect distinct modes of signaling. Sci. Signal. https://doi.org/10.1126/scisignal.aan6622.

Kenakin, T. (2011). Functional selectivity and biased receptor signaling. J. Pharmacol. Exp. Ther. *336*, 296–302.

Kerr, J.N., and Nimmerjahn, A. (2012). Functional imaging in freely moving animals. Curr. Opin. Neurobiol. *22*, 45–53.

Khanna, I.K., and Pillarisetti, S. (2015). Buprenorphine - an attractive opioid with underutilized potential in treatment of chronic pain. J. Pain Res. *8*, 859–870.

Luttrell, L.M., Maudsley, S., and Gesty-Palmer, D. (2018). Translating in vitro ligand bias into in vivo efficacy. Cell Signal. *41*, 46–55.

Manglik, A., Lin, H., Aryal, D.K., McCorvy, J.D., Dengler, D., Corder, G., Levit, A., Kling, R.C., Bernat, V., Hubner, H., et al. (2016). Structure-based discovery of opioid analgesics with reduced side effects. Nature *537*, 185–190.

McPherson, J., Rivero, G., Baptist, M., Llorente, J., Al-Sabah, S., Krasel, C., Dewey, W.L., Bailey, C.P., Rosethorne, E.M., Charlton, S.J., et al. (2010). mu-opioid receptors: correlation of agonist efficacy for signalling with ability to activate internalization. Mol. Pharmacol. *78*, 756–766.

Nagai, T., Ibata, K., Park, E.S., Kubota, M., Mikoshiba, K., and Miyawaki, A. (2002). A variant of yellow fluorescent protein with fast and efficient maturation for cell-biological applications. Nat. Biotechnol. *20*, 87–90.

Namkung, Y., Le Gouill, C., Lukashova, V., Kobayashi, H., Hogue, M., Khoury, E., Song, M., Bouvier, M., and Laporte, S.A. (2016). Monitoring G protein-coupled receptor and beta-arrestin trafficking in live cells using enhanced bystander BRET. Nat. Commun. *7*, 12178.

Olson, K.M., Lei, W., Keresztes, A., LaVigne, J., and Streicher, J.M. (2017). Novel molecular strategies and targets for opioid drug discovery for the treatment of chronic pain. Yale J. Biol. Med. *90*, 97–110.

Pradhan, A.A., Smith, M.L., Kieffer, B.L., and Evans, C.J. (2012). Ligand-directed signalling within the opioid receptor family. Br. J. Pharmacol. *167*, 960–969.

Ribas, C., Penela, P., Murga, C., Salcedo, A., Garcia-Hoz, C., Jurado-Pueyo, M., Aymerich, I., and Mayor, F., Jr. (2007). The G protein-coupled receptor kinase (GRK) interactome: role of GRKs in GPCR regulation and signaling. Biochim. Biophys. Acta *1768*, 913–922.

Scherrer, G., Imamachi, N., Cao, Y.Q., Contet, C., Mennicken, F., O'Donnell, D., Kieffer, B.L., and Basbaum, A.I. (2009). Dissociation of the opioid receptor mechanisms that control mechanical and heat pain. Cell *137*, 1148–1159.

Schmid, C.L., Kennedy, N.M., Ross, N.C., Lovell, K.M., Yue, Z., Morgenweck, J., Cameron, M.D., Bannister, T.D., and Bohn, L.M. (2017). Bias factor and therapeutic window correlate to predict safer opioid analgesics. Cell *171*, 1165–1175.e13.

Singla, N., Minkowitz, H.S., Soergel, D.G., Burt, D.A., Subach, R.A., Salamea, M.Y., Fossler, M.J., and Skobieranda, F. (2017). A randomized, Phase IIb study investigating oliceridine (TRV130), a novel micro-receptor G-protein pathway selective (mu-GPS) modulator, for the management of moderate to severe acute pain following abdominoplasty. J. Pain Res. *10*, 2413–2424.

Siuda, E.R., Carr, R., 3rd, Rominger, D.H., and Violin, J.D. (2017). Biased mu-opioid receptor ligands: a promising new generation of pain therapeutics. Curr. Opin. Pharmacol. *32*, 77–84.

Sriram, K., and Insel, P.A. (2018). G protein-coupled receptors as targets for approved drugs: how many targets and how many drugs? Mol. Pharmacol. *93*, 251–258.

Stoeber, M., Jullie, D., Lobingier, B.T., Laeremans, T., Steyaert, J., Schiller, P.W., Manglik, A., and von Zastrow, M. (2018). A genetically encoded biosensor reveals location bias of opioid drug action. Neuron *98*, 963–976.e5.

Suzuki, J., and El-Haddad, S. (2017). A review: fentanyl and non-pharmaceutical fentanyls. Drug Alcohol Depend. *171*, 107–116.

Urs, N.M., Gee, S.M., Pack, T.F., McCorvy, J.D., Evron, T., Snyder, J.C., Yang, X., Rodriguiz, R.M., Borrelli, E., Wetsel, W.C., et al. (2016). Distinct cortical and striatal actions of a beta-arrestin-biased dopamine D2 receptor ligand reveal unique antipsychotic-like properties. Proc. Natl. Acad. Sci. U S A *113*, E8178–E8186.

Wacker, D., Stevens, R.C., and Roth, B.L. (2017). How ligands illuminate GPCR molecular pharmacology. Cell *170*, 414–427.

Williams, J.T., Ingram, S.L., Henderson, G., Chavkin, C., von Zastrow, M., Schulz, S., Koch, T., Evans, C.J., and Christie, M.J. (2013). Regulation of mu-opioid receptors: desensitization, phosphorylation, internalization, and tolerance. Pharmacol. Rev. *65*, 223–254.

Zaki, P.A., Keith, D.E., Jr., Brine, G.A., Carroll, F.I., and Evans, C.J. (2000). Ligand-induced changes in surface mu-opioid receptor number: relationship to G protein activation? J. Pharmacol. Exp. Ther. *292*, 1127–1134.

Zhou, L., and Bohn, L.M. (2014). Functional selectivity of GPCR signaling in animals. Curr. Opin. Cell Biol. *27*, 102–108.

ISCI, Volume *14*

Supplemental Information

Biased Signaling of the Mu Opioid Receptor Revealed in Native Neurons

Aliza T. Ehrlich, Meriem Semache, Florence Gross, Dillon F. Da Fonte, Leonie Runtz, Christine Colley, Amina Mezni, Christian Le Gouill, Viktoriya Lukasheva, Mireille Hogue, Emmanuel Darcq, Michel Bouvier, and Brigitte L. Kieffer

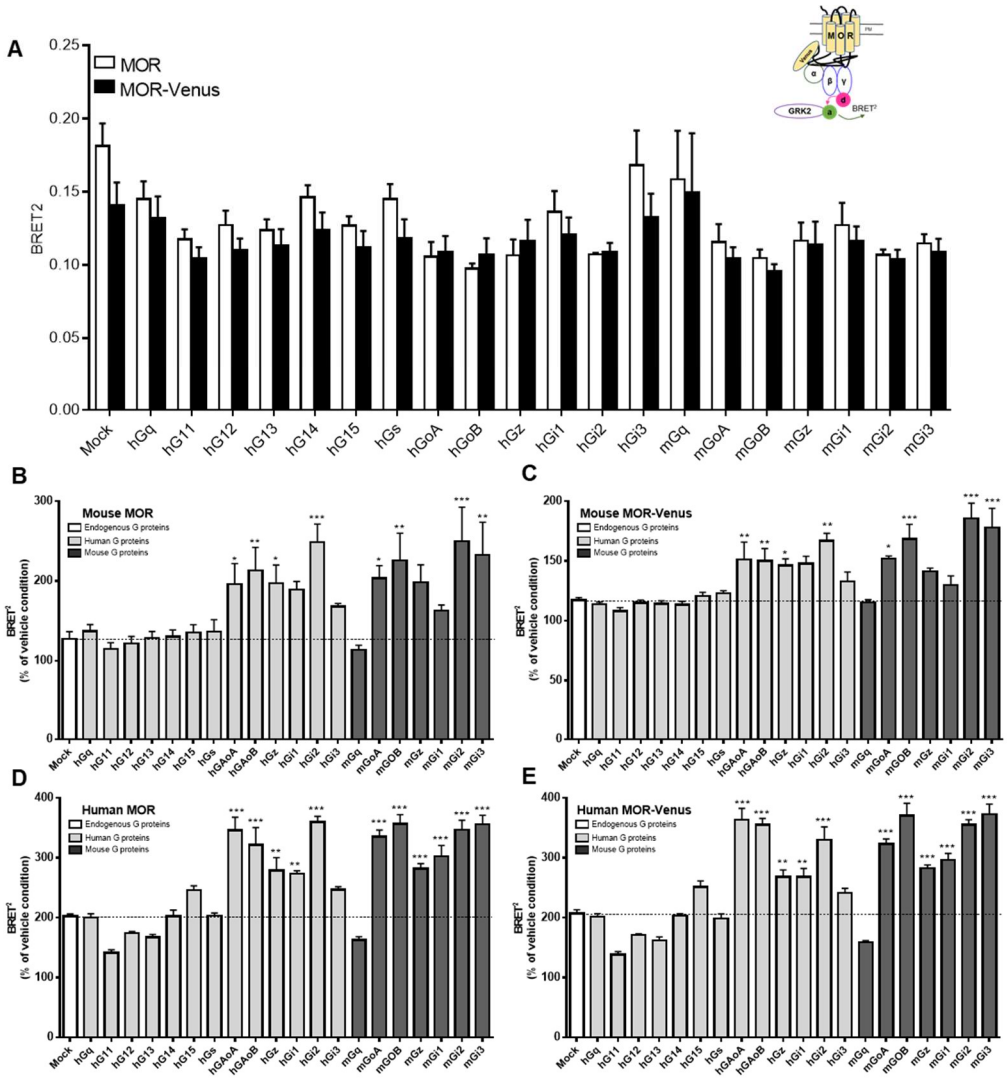

Fig. S1 Mouse and human MOR-mediated G protein activation profile. Related to Figure 1. **(A)** G protein basal activation profile of untagged MOR (white bars) versus MOR-Venus (black bars) in the absence of agonist stimulation. HEK-293 cells were co-transfected with mouse (m) MOR or MOR-Venus receptor construct, Gβ1, and $BRET^2$ sensors, human (h) Gγ3-RlucII (donor), hGRK2-GFP10 (acceptor) and either of the indicated (h) or (m) Gα subunits. Mock is a condition where cells were not co-transfected with any Gα subunit and shows MOR1-mediated activation of endogenous G proteins. No statistical significance was observed between MOR and MOR-Venus (Mann-Whitney test). **(B-D)** Following 10 minutes of stimulation with 0.3 µM of Met-Enkephalin, G protein signaling profiles are shown for untagged MOR vs. MOR-Venus, mouse **(B** and **C)** or human **(D** and **E)** receptor. For comparison, the data in **Figure 1C** is also included here in **B** and **C**. HEK-293 cells were co-transfected with (h) or (m) MOR or MOR-Venus receptor construct, Gβ1 (human and mice have identical sequences), hGγ3-RlucII (donor $BRET^2$ sensor), hGRK2-GFP10 (acceptor $BRET^2$ sensor) and either of the indicated mouse (m) or human (h) Gα subunits. Mock is a condition where cells were not co-transfected with any Gα subunit and shows transfected MOR-mediated activation of endogenous G proteins. Data are expressed as raw BRET ± SEM **(A)** or mean % of vehicle condition ± SEM **(B-E)**, one-way ANOVA *P<0.05, **P<0.001, ***P<0.0001 vs Mock condition, 3-5 replicate experiments.

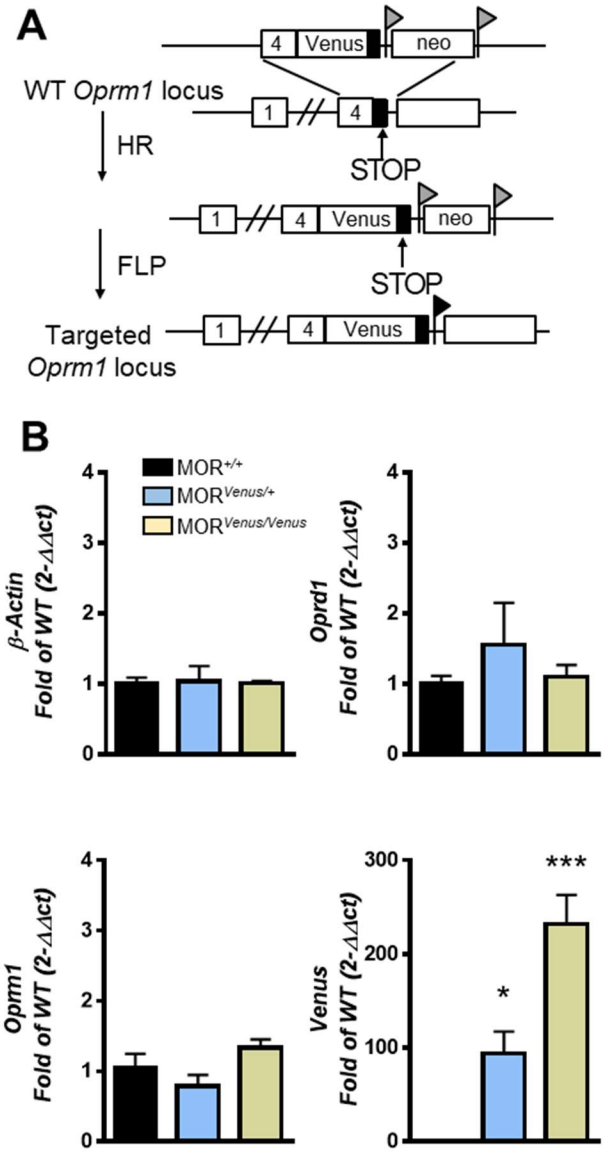

Fig. S2 MOR-Venus mouse generation and gene expression. Related to Figure 1. (**A**) Homologous recombination (HR) strategy for the construction of MOR-Venus mice. Venus cDNA was inserted in *Oprm1* exon 4, and the stop codon was replaced by a Gly-Ser-Ile-Ala-Thr- linker sequence followed by Venus encoding cDNA. The following intron contains a neomycin cassette flanked by 2 FRT sites to select positive clones. Following HR in embryonic stem cells, positive clones were microinjected into C57Bl6/N blastocytes which were crossed with FLP C57Bl6/N mice to excise *neo*. Chimeric mice were crossed with C57Bl6/N to obtain F1 heterozygous progenies. (**B**) *β-Actin*, *Oprd1* and *Oprm1* whole brain mRNA is similar across genotypes, whereas *Venus* is proportionally increased in heterozygote and homozygote animals (*n=4-6*). For one-way ANOVA, Bonferroni (multiple comparison to $MOR^{+/+}$) post-hoc test found * $P<0.05$ $MOR^{Venus/+}$ and *** $P<0.001$ $MOR^{Venus/Venus}$. All data are presented as mean of triplicates ± SEM.

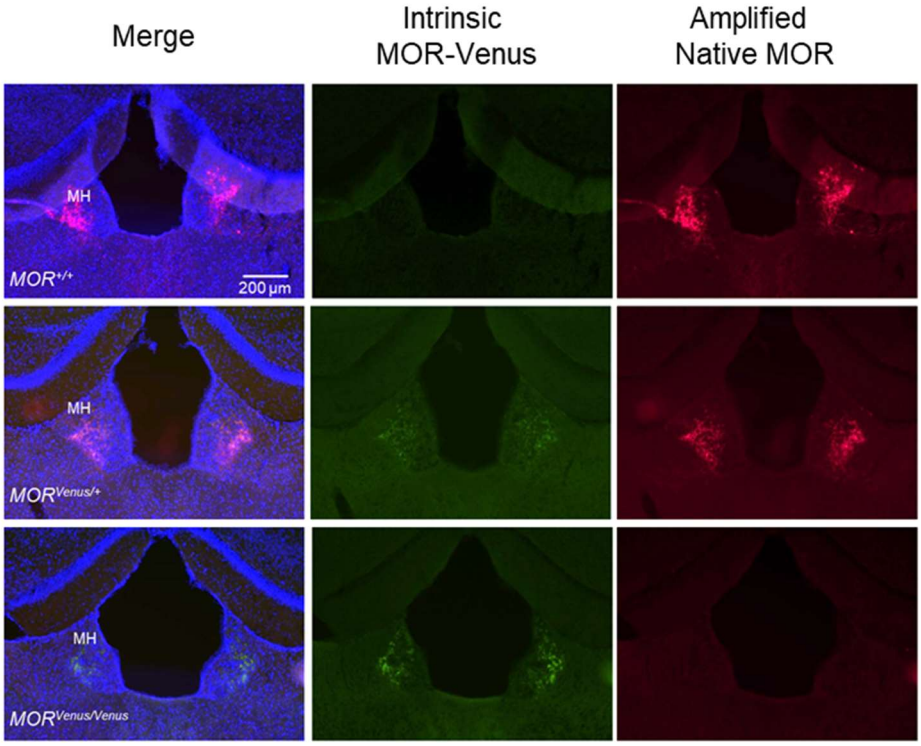

Fig. S3 MOR-Venus intrinsic fluorescence co-localization with immunodetected native MORs in *MOR*$^{Venus/+}$ mice. Related to Figure 1. MOR-Venus intrinsic fluorescence is shown in *green* channel and is weaker in *MOR*$^{Venus/+}$ than in *MOR*$^{Venus/Venus}$ knock-in animals. No signal was detected in *MOR*$^{+/+}$. Immunodetection with Anti-MOR (1:1000) followed by Alexa Fluor 594 (1:2000) show native wild-type MOR amplified signal is easily detectable in *MOR*$^{+/+}$ or partially in *MOR*$^{Venus/+}$ animals, *red* channel. Native MOR was not detected by the C-terminal epitope recognizing MOR antibody in *MOR*$^{Venus/Venus}$ knock-in animals due to the masked epitope by Venus. Merged image also contains DAPI (*blue*) to stain nuclei. Scale bar is 200 µm.

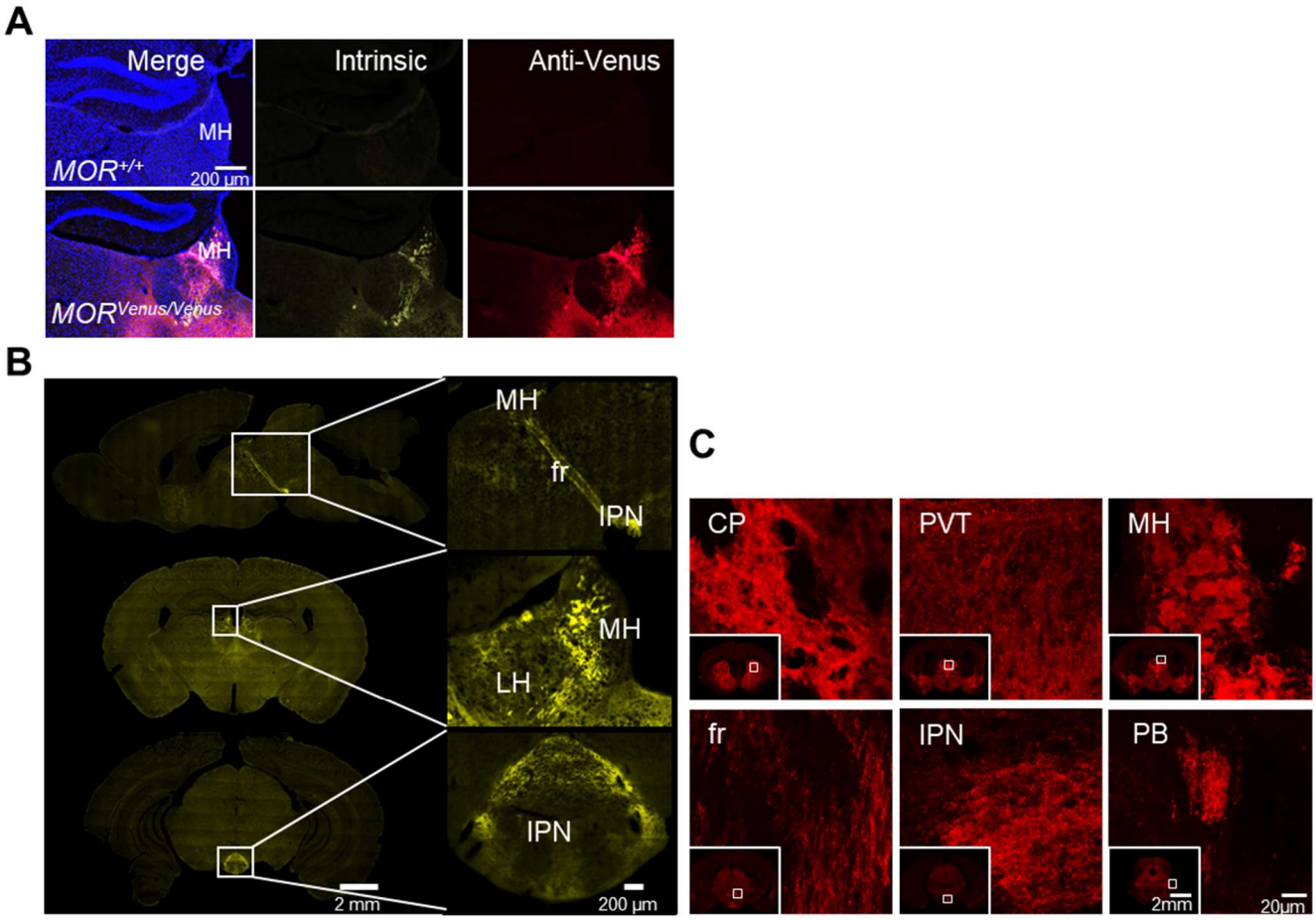

Fig. S4 Regional pattern of MOR-Venus expression in knock-in mice. Related to Figure 1. (**A**) To amplify MOR-Venus signal, brain sections were immunostained with anti-Venus (red). Epifluorescent microscopy shows MOR-Venus intrinsic fluorescence (yellow) and amplified (red) revealed co-localized signals in medial habenula (MH) neurons of *MOR*$^{Venus/Venus}$ but not *MOR*$^{+/+}$ brain sections. Merged image also contains DAPI (blue) to stain nuclei. Scale bar is 200 µm. (**B**) Slide scanner imaging of intrinsic MOR-Venus fluorescence demonstrates the expected receptor regional distribution. *Top*, a sagittal section reveals a MOR-Venus neuronal pathway that originates in the MH and extends via the fasciculus retroflexus (fr) until the interpeduncular nucleus (IPN). Macroview (*left*) scale bar is 2 mm, magnified boxed regions (*right*) scale bar is 200 µm. (**C**) Representative confocal images of mapping MOR-Venus expression (**Figure 1G** and **Table S1**) show brain areas with highest MOR expression. Scale bars for macroview insets are 2 mm, magnified views are 20 µm. Annotations: lateral habenula (LH), caudate putamen (CP), paraventricular thalamus (PVT) and parabrachial nucleus (PB).

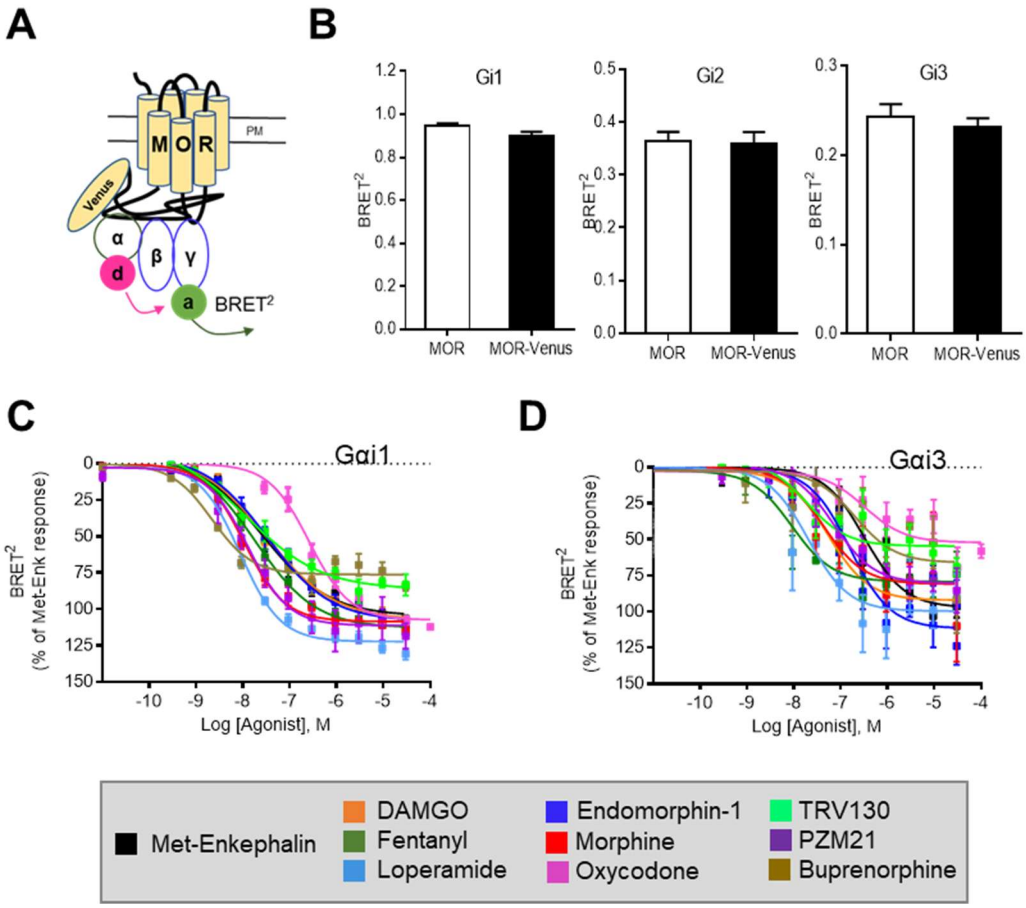

Fig. S5 G protein activation for the 10 MOR agonists in HEK-293 cells. Related to Figure 2. (**A**) Schematic representation of the BRET-based biosensor used in **B-D**. HEK-293 cells were co-transfected with MOR-Venus, Gβ1, Gγ2-GFP10 and RlucII-tagged Gαi subtypes. Cells were then stimulated 10 minutes with increasing concentrations of the indicated compound. Upon activation of the receptor, the Gαi-Rluc ((d), donor) dissociates from the βγ-GFP10 ((a), acceptor), which results in a decrease in $BRET^2$ signal. (**B**) Comparison of basal activities at Gαi1, Gαi2 and Gαi3 for untagged MOR (white bars) and MOR-Venus (black bars) using the same biosensor as in (**A**). All data are expressed as raw BRET ± SEM, no statistical significance was observed between MOR and MOR-Venus (Mann-Whitney test), 3-5 replicate experiments. (**C-D**) Concentration response curves for Gαi1 (**C**) and Gαi3 (**D**). Curves for Gαi2 are shown in **Figure 2A**. Pharmacological properties for Gαi1, Gαi2 and Gαi3 biosensors are described in **Table S2**. Data are expressed as % of Met-Enkephalin (Met-Enk) response (n= 3-7 independent experiments). All data are shown as mean ± SEM. Annotations: PM, plasma membrane.

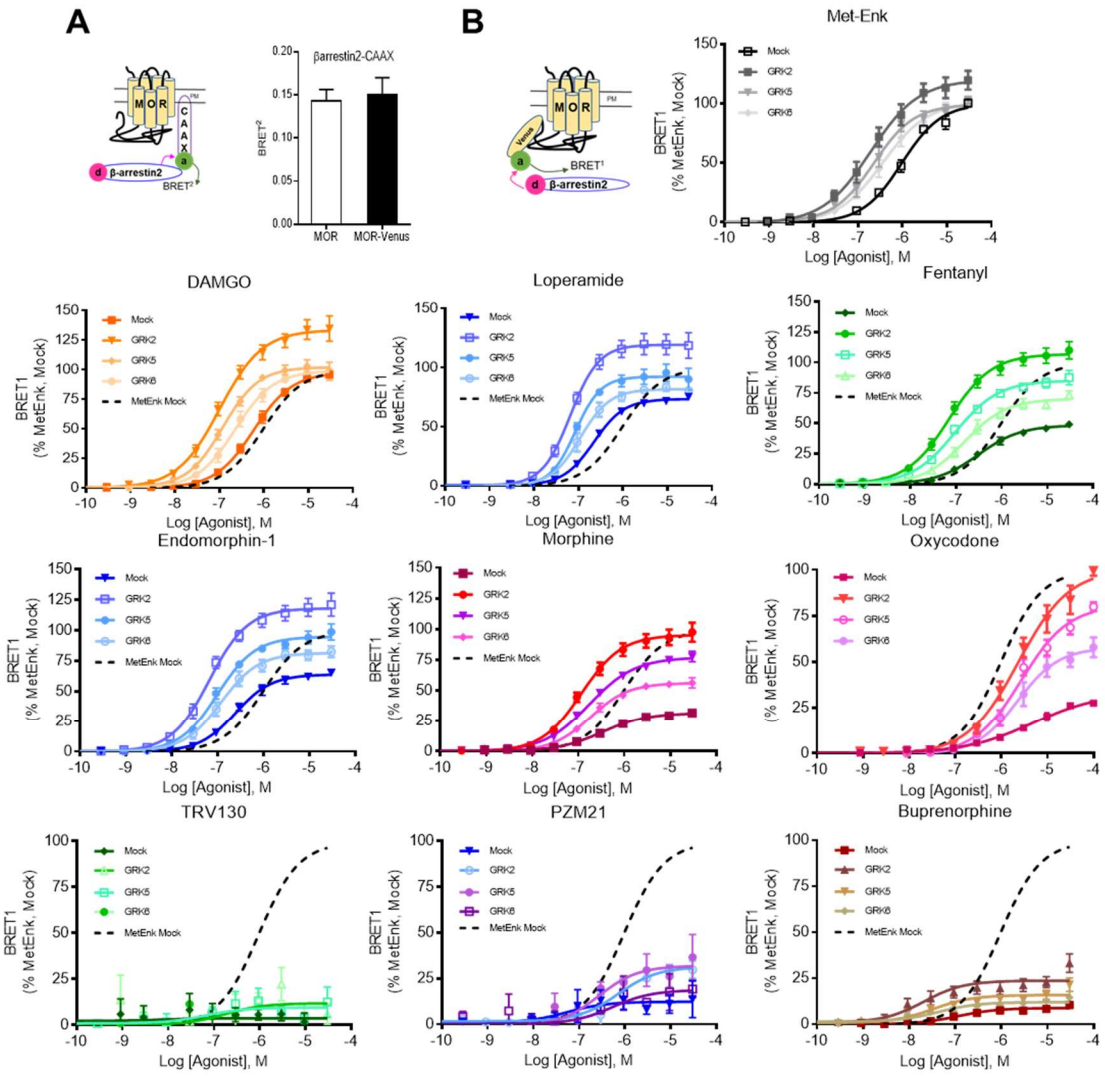

Fig. S6 βarrestin2 recruitment for the 10 MOR agonists in HEK-293 cells. Related to Figure 2. (**A**) Scheme shows the biosensor used to monitor βarr2 recruitment to the membrane. Basal activity was measured in HEK-293 cells transfected with MOR or MOR-Venus and $BRET^2$ biosensor, βarrestin2-RlucII ((d), donor) and rGFP-CAAX ((a), acceptor). Data are expressed as raw BRET ± SEM, no statistical significance was observed between MOR and MOR-Venus (Mann-Whitney test), 3-5 replicate experiments. (**B**) Scheme shows the BRET-based biosensor used to monitor βarr2 recruitment to the receptor. Upon activation of the receptor, the RlucII-tagged βarrestin2 (d) is recruited to Venus-tagged MOR (a) increasing $BRET^1$ signal. HEK-293 cells were co-transfected with MOR-Venus and βarrestin2-RlucII only (Mock) or with either GRK2, GRK5 or GRK6 and were stimulated with increasing concentrations of the indicated compounds for 10 min. Mock curves are also shown in **Figure 2B**. The pharmacological properties of the 10 compounds in the absence or presence of GRK2, GRK5 or GRK6 are summarized in **Table S3.** Data are expressed as % of Met-Enkephalin (Met-Enk) response in the absence of GRK, (n= 4-9 independent experiments). Annotations: PM, plasma membrane.

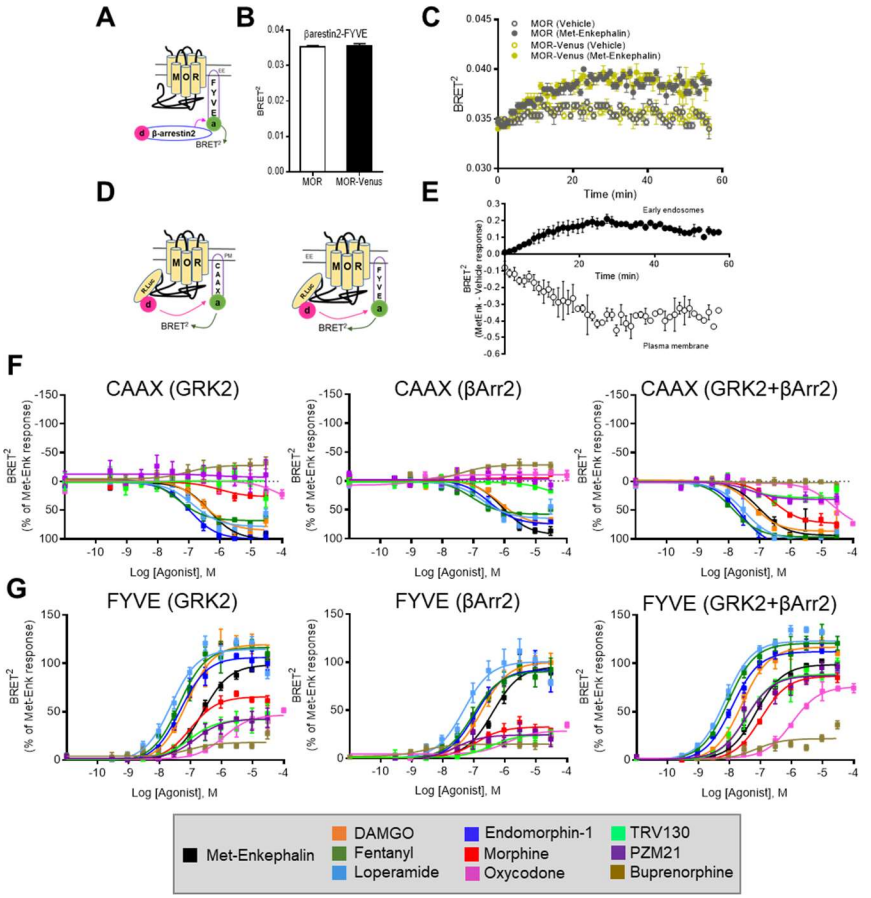

Fig. S7 Receptor trafficking for the 10 MOR agonists in HEK-293 cells. Related to Figure 2. (**A**) Schematic representation of the BRET^2-based biosensor used (**B-C**) to monitor βarrestin2 recruitment to endosomes as a surrogate for MOR internalization. HEK-293 cells were transfected with MOR or MOR-Venus and βarrestin2-RlucII ((d), donor) and FYVE-rGFP ((a), acceptor). (**B**) In the absence of agonist stimulation, basal internalization does not differ between untagged and Venus-tagged receptor (Mann-Whitney test). Data are expressed as raw BRET ± SEM, 3-5 replicate experiments. (**C**) Comparison of the internalization kinetics for MOR vs. MOR-Venus in response to 30 µM Met-Enkephalin (Met-Enk) stimulation in HEK-293 cells. Data are expressed as raw BRET ± SEM, representative experiment of 3 replicate experiments. (**D**) Schematic representation of the biosensor used in **E-G** to monitor receptor redistribution from the plasma membrane (PM) and early endosome (EE) translocation. *Left*, receptor disappearance from the PM results in a decrease of the BRET signal measured between RlucII-tagged MOR (d) and the rGFP-tagged CAAX motif (a) anchored at the PM. *Right*, localization of the receptor at the EE compartments results in an increase of the BRET signal measured between MOR-RlucII (d) and rGFP-FYVE (a) anchored to the EE. (**E**) Kinetics of MOR internalization in response to 0.3 µM Met-Enk stimulation was time-dependently monitored in HEK-293 cells co-expressing either CAAX (white circles) or FYVE (black circles) biosensors. Data are expressed as % of Met-Enk-vehicle response (**F-G**) Concentration response curves of the 10 compounds for (**F**) receptor redistribution from the PM and (**G**) receptor translocation to the EE compartments. HEK-293 cells transiently co-expressing biosensors with either GRK2, βarrestin2 or both were stimulated with increasing concentrations of the indicated compounds for 30 min. CAAX and FYVE curves without addition of GRK2 and βarrestin2 are shown in **Figure 2C** and **D**, respectively and a data table summarizing the pharmacological properties of the selected compounds is shown in **Table S4**. Data are expressed as % of Met-Enk response in the respective condition, 4-7 independent experiments).

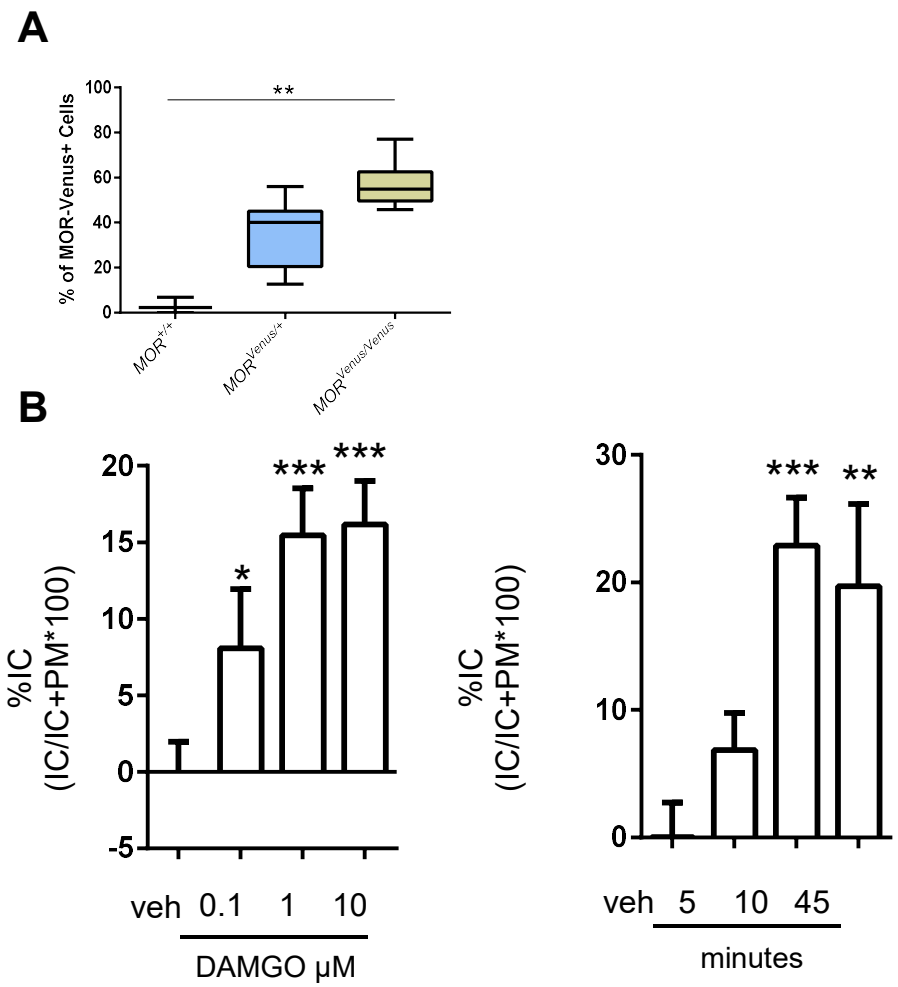

Fig. S8 MOR-Venus trafficking in dorsal root ganglia neurons. Related to Figure 2. (**A**) DRG neurons in 3-8 ganglion per genotype were counted and shown is the ratio of MOR-Venus positive to total DRG neurons. MOR-Venus positive neurons were 54% ± 5% of all dorsal root ganglia (DRG) neurons. Statistically significant differences derived from one-way ANOVA compared to wildtype (**B**) *Left*, cultured neurons derived from MOR-Venus DRG were incubated for 10 minutes with 0.1, 1, 10 µM or vehicle (veh) and MOR-Venus redistribution from plasma membrane (PM) to intracellular (IC) compartment was measured on confocal images (n= 30-37 cells) as described in the method section. Data are expressed as %IC where IC/ Total (IC+PM) and vehicle was subtracted. *Right*, neurons were treated with 1 µM DAMGO for 5, 10 or 45 minutes and compared to vehicle (45 min), (n= 17-26 cells). mean ± SEM, 2 independent experiments. Statistical significance is defined as *P<0.05, ** P <0.001, *** P <0.0001 vs vehicle in a one-way ANOVA.

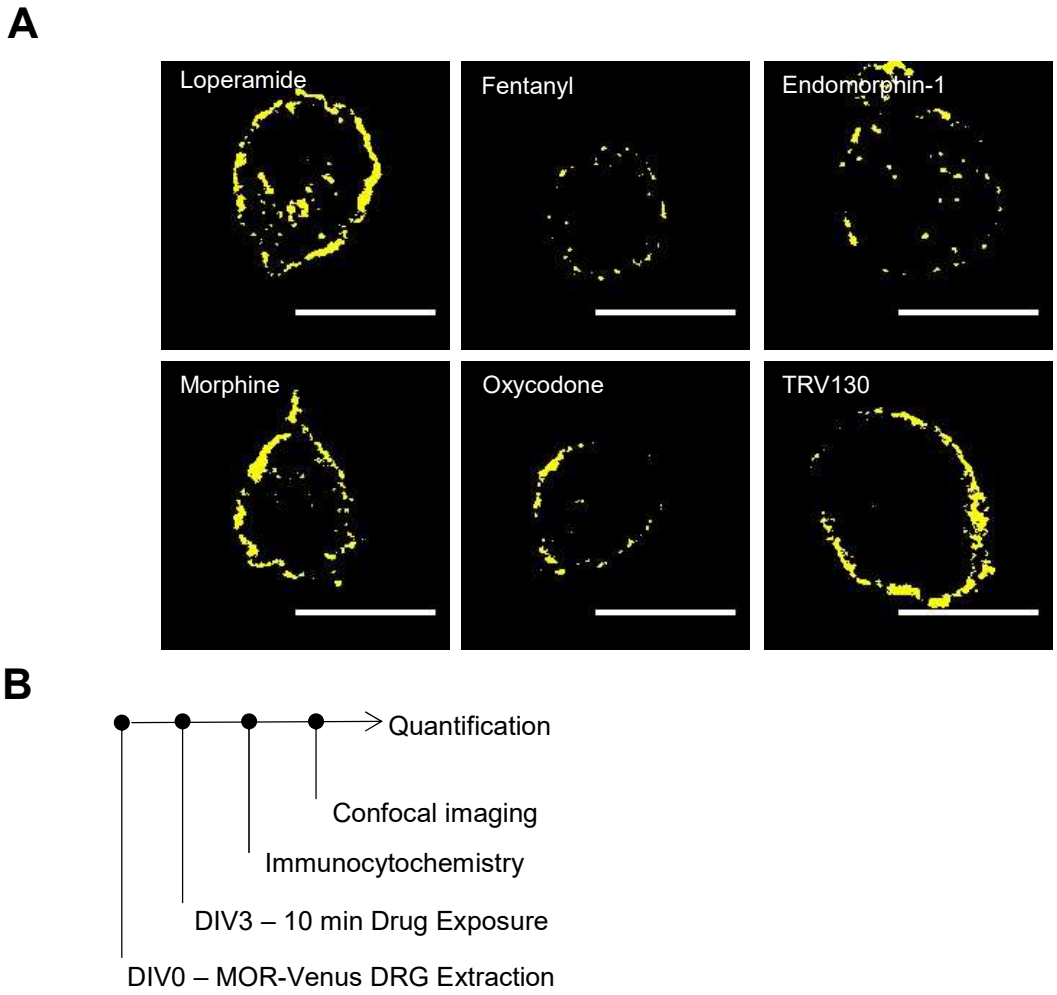

Fig. S9 Agonist mediated redistribution of MOR-Venus in DRG neurons. Related to Figure 2. Confocal imaging of MOR-Venus DRG neurons exposed to 1 μM MOR agonists for 10 minutes show alterations in receptor distribution according to the compound. (**A**) Representative confocal images of DRG neurons treated with the indicated MOR agonists. Other agonists are shown in **Figure 2E.** Scale bar 10 μm for all images. (**B**) Brief timeline of experiments beginning on the first day in vitro (DIV).

.

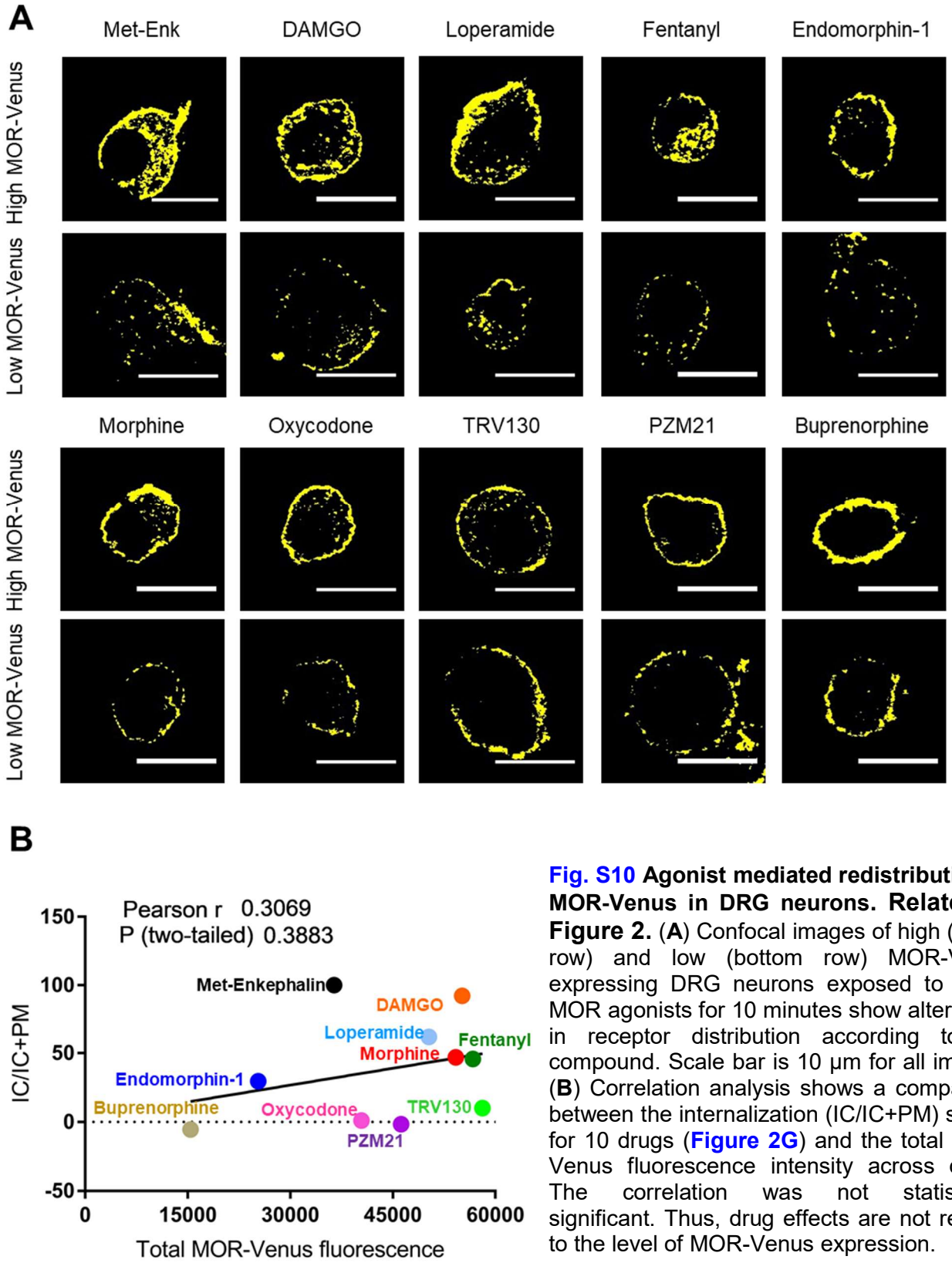

Fig. S10 Agonist mediated redistribution of MOR-Venus in DRG neurons. Related to Figure 2. (**A**) Confocal images of high (upper row) and low (bottom row) MOR-Venus expressing DRG neurons exposed to 1 μM MOR agonists for 10 minutes show alterations in receptor distribution according to the compound. Scale bar is 10 μm for all images. (**B**) Correlation analysis shows a comparison between the internalization (IC/IC+PM) scores for 10 drugs (**Figure 2G**) and the total MOR-Venus fluorescence intensity across drugs. The correlation was not statistically significant. Thus, drug effects are not relative to the level of MOR-Venus expression.

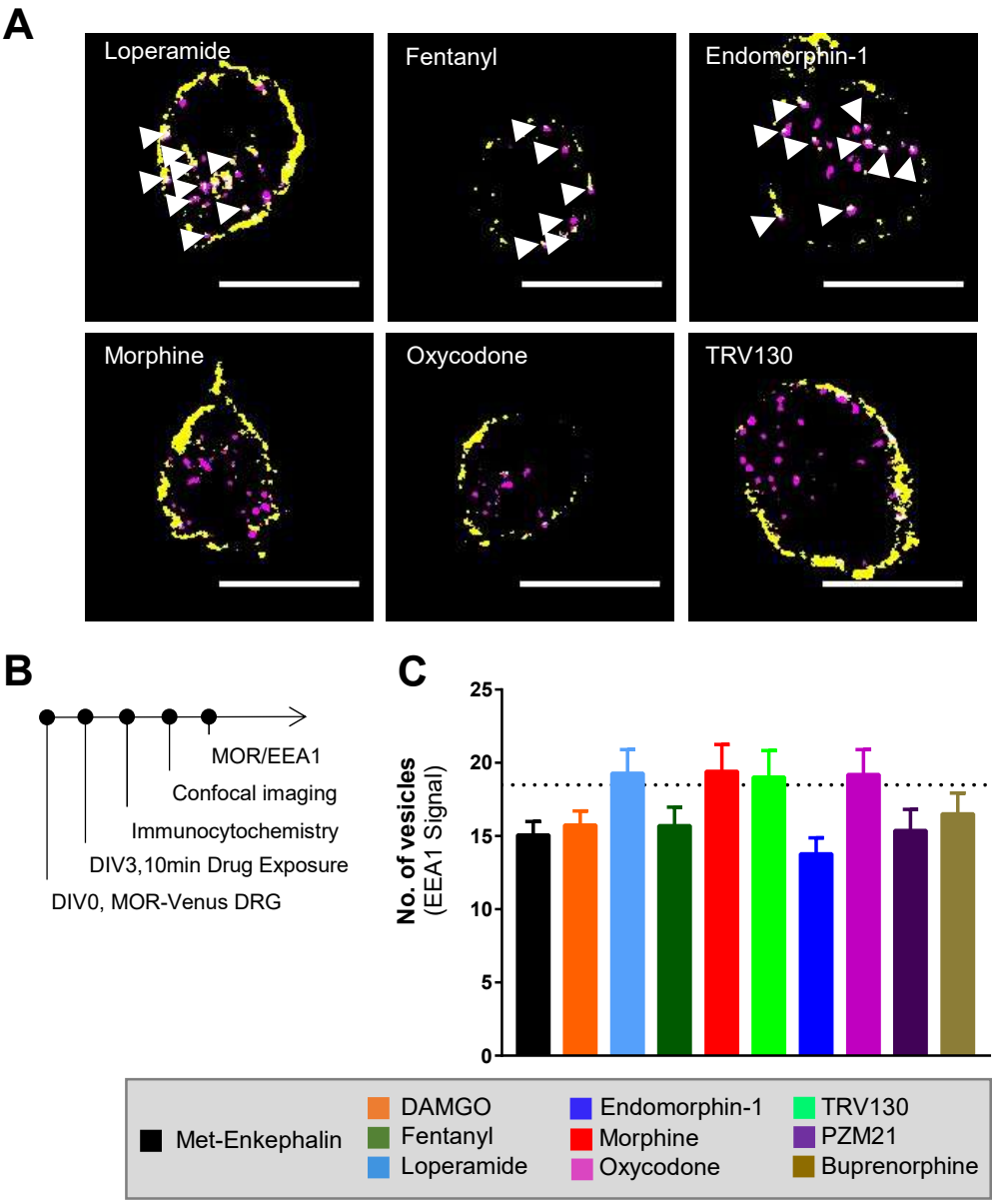

Fig. S11 MOR translocation to early endosomes in MOR-Venus DRG neurons. Related to Figure 2. Confocal imaging of MOR-Venus DRG neurons exposed to 1 μM MOR agonists for 10 minutes show receptor redistribution into early endosomes differs across compounds. (**A**) Representative confocal images are shown for the indicated MOR agonists and the other agonists are shown in **Figure 2H**. MOR-Venus signal is shown in yellow and EEA1 signals are in magenta, white arrows indicate colocalized MOR-Venus and EEA1. Scale bar 10 μm for all images. (**B**) Brief timeline of experiment is shown beginning from the first day in vitro (DIV). (**C**) Shown is the average number of EEA1 positive vesicles per DRG neuron. The broken line indicates the vesicle number in vehicle treated cells. The number of EEA1 positive vesicles did not significantly differ across treatments (one-way ANOVA, Dunn's multiple comparison test versus Met-Enk). Data presented are from 3 experiments with a total of *n=26-42* cells per drug condition. All data are presented as mean ± SEM.

Cerebrum - Cerebral Cortex	
Cortical plate	
Isocortex	
Prelimbic area	++
Infralimbic area	+
Anterior cingulate area	+
Somatosensory area	+
Somatomotor	+
Retrosplenial	+
Agranular insular	+
Olfactory Areas	
Anterior Olfactory Nucleus	+
Cortical amygdalar area	++
Hippocampal formation	
CA 1	+
CA 2	+
CA 3	+
Subiculum	+
Cortical Subplate	
Basoamygdalar nucleus	+
Endopiriform nucleus	++
Cerebrum - Cerebral Nuclei	
Striatum	
Dorsal, Caudoputamen (Patch)	+++
Ventral,Nuc. Accumbens	
Core	++
Shell	++
Striatum-like amygdalar	
Central	++
Medial	++
Anterior	++
Pallidum, medial region	
Medial septal complex	++
Triangular nucleus	++
Pallidum, caudal region	
Bed nuclei of the stria terminalis	++
Brainstem - Interbrain	
Thalamus, Polymodal association cortex	
Intralaminar, Central medial nucleus	+++
Medial group of the dorsal thalamus	+
Midline group, Paraventricular nucleus	+++
Midline group, Nucleus of reuniens	++
Epithalamus	
Medial habenula	++++
Lateral habenula	++
Hypothalamus	
Periventricular	
Dorsomedial nucleus hypothalamus	++
Lateral, Lateral hypothalamic area	++
Medial, Medial mammillary nucleus	+++
Brainstem - Midbrain	
Midbrain, sensory related	
Superior colliculus	++
Inferior colliculus	++
Midbrain, motor related	
Ventral tegmental area	++
Periaqueductal gray	++
Midbrain, behavior state related	
Substantia nigra, compact part	++
Interpeduncular Nucleus	++++
Dorsal Raphe	++
Brainstem - Hindbrain	
Pons	
sensory related	
Parabrachial Area	++++
behavioral state related	
Locus ceruleus	++
Fiber tracts	
Medial forebrain bundle system	
Cerebrum related,Fornix system	
Dorsal fornix	++
Hypothalamus related,Epithalamus	
Fasciculus retroflexus	++++

Table S1 Regional MOR-Venus expression. Related to Figure 1. Amplified MOR-Venus expression was mapped in 3-4 animals and categorized according to the Allen Brain Atlas. Areas are ranked according to degree of expression: very low (+), low (++), moderate (+++) or high (++++).

	Gαi1		Gαi2		Gαi3	
	Emax (%)	$LogEC_{50}$	Emax (%)	$LogEC_{50}$	Emax (%)	$LogEC_{50}$
Met-Enkephalin	100,0 ± 3,8	-7,61 ± 0,08	100,0 ± 5,7	-7,28 ± 0,13	100,0 ± 12,4	-6,50 ± 0,25
DAMGO	102,5 ± 3,5	-7,53 ± 0,07	97,2 ± 7,3	-7,75 ± 0,16	92,6 ± 10,7	-7,27 ± 0,25
Loperamide	125,9 ± 2,9***	-8,07 ± 0,05	109,3 ± 6,8	-7,98 ± 0,14	102,6 ± 13,7	-7,69 ± 0,28
Endomorphin-1	104,4 ± 4,0	-7,49 ± 0,08	99,2 ± 5,7	-7,71 ± 0,13	114,4 ± 12,5	-6,81 ± 0,23
Fentanyl	110,6 ± 3,4	-7,73 ± 0,07	101,5 ± 5,0	-7,90 ± 0,11	81,6 ± 10,2	-7,98 ± 0,26
Morphine	111,8 ± 2,8	-7,97 ± 0,05	103,0 ± 7,6	-7,61 ± 0,16	83,6 ± 12,3	-7,38 ± 0,32
Oxycodone	110,9 ± 3,4	-6,58 ± 0,07***	104,9 ± 6,7	-6,58 ± 0,14	68,8 ± 17,0	-4,99 ± 0,39
TRV130	85,2 ± 4,2**	-7,86 ± 0,10	85,4 ± 4,5	-7,62 ± 0,12	62,2 ± 17,9*	-6,05 ± 0,54**
PZM21	105,4 ± 7,5	-7,83 ± 0,15	105,6 ± 6,3	-7,95 ± 0,13	84,1 ± 6,7	-7,15 ± 0,19
Buprenorphine	78,5 ± 4,5***	-8,67 ± 0,10***	55,2 ± 9,9***	-8,40 ± 0,36**	65,7 ± 12,0	-6,70 ± 0,38

Table S2 Ligand-induced MOR-mediated activation of mouse Gαi proteins. Related to Figure 2. Data table summarizing the pharmacological properties of the selected compounds for Gαi1, Gαi2 and Gαi3 activation (see **Figure 2A and S5C-D**). HEK-293 cells were co-transfected with MOR-Venus receptor construct, Gβ1, Gγ2-GFP10 (acceptor $BRET^2$ sensor) and RlucII-tagged Gαi1, 2 or 3 (donor $BRET^2$ sensor). Cells were stimulated for 10 minutes with increasing concentrations of the indicated compound. Emax values are expressed as mean ± SEM % of the maximal response induced by Met-Enkephalin (Met-Enk). Potency values are expressed as $LogEC_{50}$ ± SEM (EC_{50} μM). Data are expressed as a mean of 3-7 independent experiments. *P<0.05, ** P<0.005, *** P<0.0001 vs Met-Enk condition (one-way ANOVA, followed by Dunnett post-hoc test).

A

	Mock		GRK2		GRK5		GRK6	
	Emax (%)	$LogEC_{50}$	Emax (%)	$LogEC_{50}$	Emax (%)	$LogEC_{50}$	Emax (%)	$LogEC_{50}$
Met-Enkephalin	100,0 ± 3,2	-6,07 ± 0,06	100,0 ± 2,7	-6,78 ± 0,06	100,0 ± 4,1	-6,61 ± 0,09	100,0 ± 2,7	-6,44 ± 0,05
DAMGO	98,2 ± 1,7	-6,29 ± 0,03	104,6 ± 2,3	-7,12 ± 0,05	106,7 ± 1,7	-6,99 ± 0,04	102,6 ± 2,2	-6,64 ± 0,05
Loperamide	77,1 ± 1,3***	-6,63 ± 0,03*	99,5 ± 2,2	-7,20 ± 0,05	96,1 ± 2,2	-7,11 ± 0,05	88,5 ± 2,3*	-6,94 ± 0,05
Endomorphin-1	67,4 ± 1,5***	-6,63 ± 0,05*	96,6 ± 2,4	-7,27 ± 0,05	96,6 ± 1,7	-7,11 ± ,04*	85,1 ± 2,3**	-6,92 ± 0,06
Fentanyl	49,4 ± 1,4***	-6,55 ± 0,06	86,7 ± 2,2	-7,24 ± 0,05	85,8 ± 1,8***	-7,13 ± 0,05*	71,9 ± 2,3***	-6,81 ± 0,07
Morphine	31,1 ± 0,9***	-6,48 ± 0,06	79,2 ± 1,7	-6,98 ± 0,04	76,6 ± 1,4***	-6,87 ± 0,04	54,9 ± 2,0***	-6,69 ± 0,08
Oxycodone	26,8 ± 1,0***	-5,49 ± 0,07*	75,6 ± 2,5**	-5,85 ± 0,07*	78,6 ± 3,4***	-5,72 ± 0,08**	51,9 ± 2,7***	-5,63 ± 0,10**
TRV130	4,1 ± 3,7***	-7,92 ± 1,74***	9,3 ± 3,5***	-6,70 ± 0,84	7,4 ± 2,2***	-7,13 ± 0,66	1,9 ± 7,7***	-7,73 ± 8,28
PZM21	11,6 ± 3,5***	-7,27 ± 0,62***	28,2 ± 5,2***	-5,86 ± 0,33	26,9 ± 3,0***	-6,60 ± 0,24	19,1 ± 4,7***	-6,27 ± 0,48
Buprenorphine	8,4 ± 0,5***	-7,03 ± 0,12***	19,8 ± 1,9***	-7,73 ± 0,20*	17,2 ± 1,5***	-7,49 ± 0,19***	10,5 ± 1,1***	-7,54 ± 0,21***

B

	Mock		GRK2		GRK5		GRK6	
	Emax (%)	$LogEC_{50}$	Emax (%)	$LogEC_{50}$	Emax (%)	$LogEC_{50}$	Emax (%)	$LogEC_{50}$
Met-Enkephalin	100,0 ± 3,2	-6,07 ± 0,04	98,1 ± 1,9	-6,78 ± 0,04	94,7 ± 2,9	-6,61 ± 0,06	98,2 ± 1,9	-6,44 ± 0,04
DAMGO	98,2 ± 1,7	-6,29 ± 0,03	131,6 ± 3,7***	-7,00 ± 0,06***	103,8 ± 2,3	-6,92 ± 0,04***	100,0 ± 2,4	-6,65 ± 0,05*
Loperamide	77,1 ± 1,3	-6,63 ± 0,03	125,8 ± 4,1***	-7,18 ± 0,07***	99,0 ± 3,2	-7,05 ± 0,07**	86,2 ± 2,5	-6,95 ± 0,06*
Endomorphin-1	67,4 ± 1,5	-6,63 ± 0,05	120,1 ± 3,5***	-7,18 ± 0,06***	96,6 ± 2,3**	-7,00 ± 0,05**	83,0 ± 2,5	-6,92 ± 0,06
Fentanyl	49,4 ± 1,4	-6,55 ± 0,06	106,1 ± 3,0***	-7,16 ± 0,06***	84,1 ± 1,9***	-7,03 ± 0,05**	69,9 ± 2,3**	-6,81 ± 0,07
Morphine	31,1 ± 0,9	-6,48 ± 0,06	96,3 ± 2,9***	-6,94 ± 0,06**	75,3 ± 1,4***	-6,78 ± 0,04	57,1 ± 1,4**	-6,73 ± 0,05
Oxycodone	26,8 ± 1,0	-5,49 ± 0,07	93,5 ± 3,3**	-5,72 ± 0,07	77,8 ± 2,5*	-5,63 ± 0,06	58,0 ± 2,1	-5,66 ± 0,07
TRV130	4,1 ± 3,7	-7,92 ± 1,74	12,0 ± 5,8	-6,76 ± 1,08	8,7 ± 3,2	-7,16 ± 0,77*	1,3 ± 7,5	-7,77 ± 11,56*
PZM21	11,6 ± 3,5	-7,27 ± 0,62	29,9 ± 4,0	-6,15 ± 0,25*	33,4 ± 4,6	-6,58 ± 0,28	18,7 ± 5,5	-6,27 ± 0,57
Buprenorphine	8,4 ± 0,5	-7,03 ± 0,12	22,9 ± 2,4***	-7,68 ± 0,22	15,3 ± 1,3**	-7,48 ± 0,18	10,7 ± 1,1	-7,36 ± 0,21

Table S3 Ligand-induced MOR-mediated activation of βarrestin2 recruitment. Related to Figure 2. Data table summarizing the pharmacological properties of the selected compounds for βarr2 recruitment (see **Figure 2B and S6B**). For βarr2 recruitment, cells were co-transfected with MOR-Venus receptor (acceptor $BRET^1$ sensor) and βarrestin2-RlucII construct (donor $BRET^1$ sensor). Cells were stimulated 10 minutes with increasing concentrations of the indicated compound. (**A**) Emax values are expressed as mean ± SEM % of the maximal response induced by Met-Enkephalin (Met-Enk) for each assay. Statistical significance is shown for indicated drug vs Met-Enk condition (one-way ANOVA, followed by Dunnett post-hoc test). (**B**) Emax values are expressed as mean ± SEM % of the maximal response induced by Met-Enk in absence of GRK overexpression (Mock condition). Statistical significance is shown for indicated drug vs Met-Enk, Mock condition (one-way ANOVA, followed by Dunnett post-hoc test). (**A-B**) * $P<0.05$, ** $P<0.005$, *** $P<0.0001$. Potency values are expressed as $LogEC_{50}$ ± SEM (EC_{50} μM). Data are expressed as a mean of 3-7 independent experiments).

	Mock		GRK2		βarrestin2		GRK2+ βarrestin2	
	Emax (%)	$LogEC_{50}$	Emax (%)	$LogEC_{50}$	Emax (%)	$LogEC_{50}$	Emax (%)	$LogEC_{50}$
Met-Enkephalin	100,0 ± 12,4	-5,75 ± 0,23	100,0 ± 4,3	-6,33 ± 0,08	100,0 ± 4,8	-6,08 ± 0,09	100,0 ± 5,4	-7,01 ± 0,12
DAMGO	102,7 ± 23,0	-5,43 ± 0,37	86,8 ± 5,3	-6,52 ± 0,12	80,7 ± 4,4	-6,16 ± 0,11	94,7 ± 7,7	-7,23 ± 0,18
Loperamide	59,7 ± 11,8	-6,49 ± 0,44	76,9 ± 5,5	-6,88 ± 0,15	66,1 ± 5,7	-6,71 ± 0,19	106,0 ± 5,2	-7,51 ± 0,11
Endomorphin-1	71,7 ± 13,7	-5,51 ± 0,33	99,5 ± 3,6	-6,98 ± 0,08	80,0 ± 4,2	-6,49 ± 0,11	120,6 ± 5,3	-7,62 ± 0,10
Fentanyl	37,2 ± 7,8	-6,42 ± 0,49	72,3 ± 2,6	-7,34 ± 0,08	61,1 ± 3,6	-7,05 ± 0,13	104,1 ± 2,3	-7,87 ± 0,05
Morphine	-26,9 ± 11,3***	-7,65 ± 0,94***	25,9 ± 5,0***	-6,02 ± 0,35	-5,1 ± 3,2***	-7,24 ± 1,36	78,0 ± 3,5	-6,53 ± 0,10
Oxycodone	-41,8 ± 12,0***	-6,92 ± 0,67	43,9 ± 61,1***	-4,08 ± 1,16	-18,6 ± 6,6***	-8,64 ± 0,65***	85,1 ± 15,3	-4,64 ± 0,22***
TRV130	-90,1 ± 36,9**	-5,04 ± 0,55	-2,4 ± 8,3***	-7,53 ± 7,19	30,3 ± 34,3***	-4,59 ± 0,97	29,7 ± 4,2**	-7,35 ± 0,32
PZM21	-35,3 ± 8,9**	-6,75 ± 0,58	5,1± 12,5***	-6,14 ± 4,56	-1,2 ± 6,0***	-7,47 ± 11,43*	32,9 ± 4,7**	-7,29 ± 0,32
Buprenorphine	-72,7 ± 13,0***	-7,37 ± 0,42**	-23,5 ± 5,9***	-7,05 ± 0,52	-27,9 ± 3,5***	-7,37 ± 0,28	2,7 ± 2,8**	-7,95 ± 2,27*

Table S4 Ligand-induced MOR internalization (CAAX assay). Related to Figure 2. Data table summarizing the pharmacological properties of the selected compounds for receptor disappearance from plasma membrane (see **Figure 2C and S7F**). HEK-293 cells were co-transfected with MOR-RlucII (donor $BRET^2$ sensor) and CAAX-rGFP for plasma membrane localization (acceptor $BRET^2$ sensors). HEK-293 cells were stimulated 30 minutes with increasing concentrations of the indicated compound. Emax values are expressed as mean ± SEM % of the maximal response induced by Met-Enkephalin (Met-Enk). Potency values are expressed as $LogEC_{50}$ ± SEM (EC_{50} μM). Data are expressed as a mean of 3-7 independent experiments. * P<0.05, ** P<0.005, *** P<0.0001 vs Met-Enk condition (one-way ANOVA, followed by Dunnett post-hoc test).

	Mock		GRK2		βarrestin2		GRK2+ βarrestin2	
	Emax (%)	$LogEC_{50}$	Emax (%)	$LogEC_{50}$	Emax (%)	$LogEC_{50}$	Emax (%)	$LogEC_{50}$
Met-Enkephalin	100,0 ± 3,8	-6,00 ± 0,07	100,0 ± 2,4	-6,62 ± 0,05	100,0 ± 4,0	-6,39 ± 0,08	100,0 ± 2,3	-7,14 ± 0,05
DAMGO	106,9 ± 5,7	-6,52 ± 0,11	122,2 ± 5,5	-7,13 ± 0,09	106,3 ± 3,9	-6,74 ± 0,08	119,5 ± 3,3*	-7,60 ± 0,06
Loperamide	105,1 ± 4,9	-7,00 ± 0,10	116,8 ± 5,0	-7,63 ± 0,09*	106,2 ± 5,8	-7,33 ± 0,12**	125,1 ± 5,0**	-8,15 ± 0,08
Endomorphin-1	77,7 ± 5,2	-6,71 ± 0,14	109,5 ± 4,5	-7,33 ± 0,09	98,5 ± 4,8	-6,96 ± 0,11	114,9 ± 3,3	-7,92 ± 0,06
Fentanyl	72,5 ± 4,9	-6,83 ± 0,14	118,8 ± 4,7	-7,37 ± 0,08	95,5 ± 5,2	-7,03 ± 0,12	122,8 ± 5,5*	-8,04 ± 0,09
Morphine	31,8 ± 5,6***	-9,00 ± 0,29**	66,6 ± 2,4***	-7,01 ± 0,07	34,3 ± 2,6***	-6,92 ± 0,17	89,0 ± 2,3	-6,99 ± 0,05
Oxycodone	18,6 ± 3,3***	-6,72 ± 0,36	46,2 ± 3,8***	-5,94 ± 0,16	25,3 ± 2,7***	-5,83 ± 0,22	75,6 ± 2,5**	-5,98 ± 0,07*
TRV130	11,2 ± 3,0***	-7,48 ± 0,57	41,4 ± 4,7***	-7,03 ± 0,24	25,2 ± 2,4***	-6,45 ± 0,20	90,3 ± 4,4	-7,47 ± 0,10
PZM21	15,3 ± 2,7***	-6,96 ± 0,37	41,3 ± 3,9***	-6,83 ± 0,20	27,1 ± 4,6***	-7,58 ± 0,37*	88,1 ± 5,0	-7,47 ± 0,12
Buprenorphine	11,3 ± 2,9***	-7,78 ± 0,53**	14,4 ± 2,8***	-7,02 ± 0,41***	13,3 ± 3,0***	-8,62 ± 0,43***	22,4 ± 3,2***	-7,16 ± 0,30

Table S5 Ligand-induced MOR translocation to early endosomes (FYVE assay). Related to Figure 2. Data table summarizing the pharmacological properties of the selected compounds for receptor localization at the early endosome (EE) compartments (see **Figure 2D and S7G**). HEK-293 cells were co-transfected with MOR-RlucII (donor $BRET^2$ sensor) and rGFP-FYVE, for EE localization (acceptor $BRET^2$ sensors). HEK-293 cells were stimulated 30 minutes with increasing concentrations of the indicated compound. Emax values are expressed as mean ± SEM % of the maximal response induced by Met-Enkephalin (Met-Enk). Potency values are expressed as $LogEC_{50}$ ± SEM (EC_{50} μM). Data are expressed as a mean of 3-7 independent experiments. * $P<0.05$, ** $P<0.005$, *** $P<0.0001$ vs Met-Enk condition (one-way ANOVA, followed by Dunnett post-hoc test).

	Minimum	Maximum	Lower 95% CI of mean	Upper 95% CI of mean	Adjusted P Value	Significant
Met-Enkephalin	-110.6	322.6	65.28	134.7		
DAMGO	-75.94	323.1	56.69	127.8	>0.99	ns
Loperamide	-110	205.7	31.38	92.27	>0.99	ns
Endomorphin-1	-107.2	258.3	2.041	57.24	0.01	*
Fentanyl	-105.2	218.7	24.34	67.04	0.16	ns
Morphine	-108	318.9	20.34	73.53	0.55	ns
Oxycodone	-110.6	105.9	-23.77	25.96	<0.001	***
TRV130	-87.59	152.6	-15.97	36.04	0.005	**
PZM21	-110.6	128.8	-23.1	19.83	<0.001	***
Buprenorphine	-110.6	87.82	-22.78	11.83	<0.001	***

Table S6 Table of statistics for MOR-Venus redistribution. Related to Figure 2. Data table summarizes the selected compound's statistics for the MOR-Venus redistribution assay in DRGs (see **Figure 2G**). Table includes column statistics (Minimum, Maximum, and 95% confidence intervals (CI) of mean). Shown in the far right two columns are the results of a one-way ANOVA Kruskal-Wallis test (Kruskal-Wallis statistic = 52.22) and Dunn's multiple comparisons test, * P<0.05, ** P<0.01, *** P<0.001 vs. Met-Enkephalin condition.

	Minimum	Maximum	Lower 95% CI of mean	Upper 95% CI of mean	Adjusted P Value	Significant
Met-Enkephalin	-169.5	275.1	63.07	136.9		
DAMGO	-211.3	332.4	50.16	155.2	>0.9999	ns
Loperamide	-180.2	262.5	51.81	130.1	>0.9999	ns
Endomorphin-1	-211.3	282.9	9.39	89.61	0.7324	ns
Fentanyl	-211.3	332.4	55.83	122.9	>0.9999	ns
Morphine	-125.5	278	38.58	117.9	>0.9999	ns
Oxycodone	-211.3	305.4	-13.82	73.7	0.2322	ns
TRV130	-154.1	332.4	30.62	107.7	>0.9999	ns
PZM21	-211.3	212.5	-47.61	46.82	0.0304	*
Buprenorphine	-211.3	133.8	-51.67	21.15	0.0006	***

Table S7 Table of statistics for MOR-Venus co-localization with EEs. Related to Figure 2. Data table summarizes the selected compound's statistics for the MOR-Venus translocation to early endosomes (EE) assay in DRGs (**Figure 2J**). Table includes column statistics (Minimum, Maximum, and 95% confidence intervals (CI) of mean). Shown in the far right two columns are the results of a one-way ANOVA Kruskal-Wallis test (Kruskal-Wallis statistic = 32.73) and Dunn's multiple comparisons test, * $P<0.05$, *** $P<0.001$ vs. Met-Enkephalin condition.

	Gαi2 vs βarrestin2			Gαi2 vs EE		
	ΔΔLogR	SEM	Bias	ΔΔLogR	SEM	Bias
Met-Enkephalin	0	0,271	ns	0	0,28	ns
DAMGO	0,263	0,193	ns	-0,463	0,211	ns
Loperamide	0,659	0,193	ns	-0,517	0,216	ns
Endomorphin-1	0,731	0,192	ns	0,113	0,214	ns
Fentanyl	1,657	0,204	Gi2	0,448	0,225	ns
Morphine	1,997	0,198	Gi2	1,531	0,227	Gi2
Oxycodone	1,89	0,205	Gi2	1,703	0,26	Gi2
TRV130	4,023	0,462	Gi2	2,615	0,404	Gi2
PZM21	3,234	0,267	Gi2	2,706	0,337	Gi2
Buprenorphine	2,853	0,192	Gi2	1,806	0,219	Gi2

Table S8 Estimate of bias. Related to Figure 3. LogR coefficients were normalized to the Met-Enkephalin to generate ΔLogR ratios which were then used to calculate ΔΔLogR ratios. Bias was calculated between MOR-mediated Gαi2 activation and either βarrestin2 recruitment or MOR localization at the early endosome compartments (EE). Data are expressed as ΔΔLogR ratio ± SEM. The column 'Bias' indicates whether the difference in bias was statistically significant towards either of the pathways compared to Met-Enkephalin. A *P* value <0.05 was considered as significant. 'ns' is otherwise indicated (One-sample *t* test).

TRANSPARENT METHODS

Drugs

The following compounds were used in this study: Dimethyl Sulfoxide (DMSO) (Sigma-Aldrich, St. Louis, Missouri), [D-Ala^2, NMe-Phe^4, Gly-ol^5]-enkephalin (DAMGO) (Tocris Bioscience, United Kingdom), loperamide (Sigma-Aldrich), Endomorphin-1, [N-C^{2}H$_3$] Morphine, Fentanyl-HCl, Buprenorphine-HCl, Oxycodone-HCl, were all obtained from NIDA Drug inventory supply and control system (RTI International, Research Triangle Park, North Carolina). [Met^5] Enkephalin acetate salt hydrate was purchased from Sigma-Aldrich. TRV130 and PZM21 was kindly provided by Alkermes.

Plasmids

Plasmids encoding all the different non-tagged human G proteins used in this study were purchased from the Missouri University of Science and Technology (www.cdna.org). Non-tagged mouse G proteins were either PCR-amplified using a Riken mouse cDNA book (Kawai & Hayashizaki, 2003) or synthesized (GeneART, ThermoFisher). All the G proteins were subcloned into pcDNA3.1(+) vector. Human (h) and mouse (m) MOR coding sequences were PCR-amplified and subcloned into pLVXi2P vector (Clontech, Mountain View, CA, USA) and pIRES vector (Invitrogen, Carlsbad, CA), respectively, using Gibson assembly (NEB, Ipswich, MA, USA). Protein sequence was optimized by the addition of a signal peptide (SP) (MKTIIALSYIFCLVFA) at the N-terminal domain sequence of the receptors. The Venus tag sequence was added to the C-terminus of mSP-MOR construct, through a short 5 amino acid linker (GSIAT). To generate mMOR-RlucII, mMOR coding sequence was PCR-amplified and inserted into pcDNA3.1/hygro(+)GFP10-RlucII vector (Leduc et al, 2009) after BamH1/Nhe1 digestion. The hSP-MOR coding sequence was PCR-amplified from pLVXi2P-SP-hMOR and subcloned into pIRES-Venus plasmid using Gibson assembly, removing the stop codon. GFP10 tag sequence was linked to the N-terminus of hGRK2 through a 7-amino acid linker (GSAGTGG) and GRK2-GFP10 was subcloned into pcDNA3.1 vector. hGγ3 coding sequence was fused in frame to the humanized Renilla luciferase II (RlucII) at its C-terminus and subcloned into pcDNA3.1 vector. RlucII-tagged mMOR, mGαi and mβ-arrestin2 were constructed by PCR-amplifying RlucII coding sequence and inserting it into pcDNA3.1(+) plasmid expressing the respective protein using Gibson assembly. mGγ2-GFP10 was generated by subcloning the GFP10-tag sequence into pcDNA3.1-mGγ2. rGFP-CAAX and rGFP-FYVE BRET biosensor constructs were generated as previously described (Namkung et al, 2016).

HEK-293 cell culture, transfection and BRET measurement

HEK-293 (Namkung et al, 2016) cells were maintained in Dulbecco's modified Eagle's medium (DMEM) supplemented with 10% fetal bovine serum and 100 U/mL penicillin/streptomycin (Wisent, Saint-Jean-Baptiste, Canada) in a 37°C humidified incubator with a 5% CO_2 atmosphere. Two days prior to experiments, cells were trypsinized (Trypsin, Wisent) and 35,000 cells were transfected with 100 ng of total DNA containing the appropriate expression vectors/biosensors. The total quantity of DNA was completed at 100 ng with salmon sperm DNA (Invitrogen). Transfection was performed using the transfecting agent polyethylenimine 25 kD

linear (PEI; Polysciences, Warrington, PA) at a ratio of 3:1 PEI/DNA. Cells were then immediately plated onto poly-ornithine (Sigma-Aldrich) coated 96-well white culture plates (PerkinElmer, Waltham, MA). Forty-eight hours post-transfection, cells were washed twice with phosphate-buffered saline (PBS) then incubated 1 hour at 37°C in Tyrode buffer (137 mM NaCl, 0.9 mM KCl, 1 mM $MgCl_2$, 1 1.9 mM $NaHCO_3$, 3.6 mM NaH_2PO_4, 25 mM HEPES, 5.5 mM Glucose and 1 mM $CaCl_2$, pH 7.4). Cells were then treated with the ligands. Compounds were initially dissolved in DMSO to generate a stock solution and then diluted in Tyrode buffer to the working concentrations as indicated. Bioluminescence resonance energy transfer (BRET) was then measured between RlucII (BRET energy donor) and either Venus ($BRET^1$ energy acceptor), GFP10 ($BRET^2$ energy acceptor) or rGFP (enhanced bystander ebBRET acceptor)–tagged proteins. BRET values were read for 1 second per well using a Mithras™ LB940 Multimode Microplate Reader (Berthold Technologies, Bad Wildbad, Germany) for single dose and concentration-response curves or a Tristar®LB942 Multimode Microplate Reader (Berthold Technologies) for kinetics measurements. $BRET^1$, $BRET^2$ and ebBRET values were obtained by calculating the ratio of the light emitted by the energy acceptor over the light emitted by the energy donor (donor 480 ± 20 nm/acceptor 530 ± 20 nm for $BRET^1$ and 410 ± 70 nm/acceptor 515 ± 20 nm for $BRET^2$). Data were collected using the MicroWin 2000 software (Berthold Technologies).

G protein Activation in HEK-293 cells

For the G protein activation assay, cells were transfected with plasmids encoding either human (h)MOR, hMOR-Venus, mouse (m)MOR or mMOR-Venus. In **Figure 1C** and **Figures S1A-S1E**, cells were co-transfected with human/mouse Gβ1, human/mouse Gγ3-RlucII and human GRK2-GFP10 along with the indicated Gα subunits to measure the activation of the Gα proteins indirectly via the release of Gβγ-Rluc that can then interact with GRK2-GFP10, resulting in a BRET increase. Mock is a condition where cells were not transfected with any of the tested Gα proteins and reflects the background endogenous response. For **Figure 1B** and **Figure S5**, the activation was assessed by directly measuring the separation between Gα and Gβγ in cells co-transfected with plasmids encoding mMOR-Venus or mMOR and mGβ1, mGγ2-GFP10 and the RlucII-tagged Gα subunits as indicated. Cells were stimulated 10 minutes with the indicated concentrations of agonists except for basal activity measured in the absence of agonist (**Figure S5B**). In all cases G protein activation was measured using $BRET^2$ filter set.

βarrestin2 recruitment and receptor trafficking in HEK-293 cells

Cells were transfected with mMOR-Venus and βarrestin2-RlucII constructs with (**Figure S6B**) or without (**Figure 2B** and **Figure S6B**) hGRK2, hGRK5 or hGRK6. Cells were stimulated 10 minutes with the indicated concentrations of agonists and βarrestin2 recruitment was measured using $BRET^1$ filters set. Receptor redistribution and localization at the early endosome compartments was assessed by ebBRET in cells expressing mMOR-RlucII and either rGFP-CAAX (plasma membrane localization) or rGFP-FYVE (early endosome compartment) in the presence (**Figure S7F-S7G**) or absence (**Figure 2C-2D**) of hGRK2 and hβarrestin2. Cells were stimulated with the selected compounds as indicated and translocation was assessed using $BRET^2$ filter set. For basal activity comparison between mMOR and mMOR-Venus, cells were transfected with either βarrestin2-RlucII and rGFP-CAAX constructs to assess βarrestin2

recruitment (**Figure S6A**) or βarrestin2-RlucII and rGFP-FYVE constructs as a surrogate for receptor trafficking (**Figure S7B**), along with either mMOR or mMOR-Venus constructs. Both measurements were done using BRET^2 filter set.

Analysis of concentration-response curves

All the curves generated for the different pathways were fitted and analyzed using the nonlinear curve fitting equations in GraphPad Prism (v7.0, GraphPad Software, Inc, San Diego, CA, USA) to estimate the pEC_{50} values.

To illustrate data from both HEK-293 cells and native neurons in radial graphs (**Figure 3**), drug overall efficiency obtained from concentration-response curves (in HEK-293 cells) was estimated by calculating $Log(\Delta Emax/EC_{50})$ ratios for each compound and normalized to Met-Enkephalin using the formula $Log\ (\Delta Emax/EC_{50})_{compound} - Log(\Delta Emax/EC_{50})_{Met\text{-}Enkephalin}$. The anti-logs were then calculated for drug responses in HEK-293 cells and responses were normalized to fit a scale of -1 to +1 using the formula (compound – Met-Enkephalin)/(compound + Met-Enkephalin). To illustrate responses in native neurons together with HEK-293 cells the % of Met-Enkephalin responses (**Figure 2G** or **2J**) were normalized as ((compound/Met-Enkephalin)-Met-Enkephalin) thus, Met-Enkephalin response is set to 0. For both HEK-293 cells and native neurons positive and negative values denote a better or a lower response as compared to Met-Enkephalin, respectively.

To calculate bias, ligand signaling efficiency was also quantified using the operational model of agonism and the transduction ratios (τ/KA) were determined using the following equations, as previously described (Black & Leff, 1983; Kenakin & Christopoulos, 2013; Nagi & Pineyro, 2016; van der Westhuizen et al, 2014):

$$E = \text{Basal} + \frac{(E_m - \text{Basal})}{1 + \left(\frac{\left(\frac{[A]}{10^{\log K_A}} + 1\right)}{10^{\log R} \times [A]}\right)^n} \qquad \text{(Eq. 1)}$$

E is the effect of the ligand, [A] is the concentration of the agonist, E_m is the maximal response, Basal is the response level in the absence of agonist, $Log K_A$ is the logarithm of the functional equilibrium dissociation constant of the agonist, n is the slope of the transducer function that links occupancy to response and LogR is the logarithm of the "transduction coefficient" (or "transduction ratio"), τ/K_A. τ is an index of the coupling efficiency of the agonist (efficacy).

For each of the tested compounds, the activity was compared to Met-Enkephalin response for a given signaling pathway using the following equation:

$\Delta log(\tau/K_A) = log\ (\tau/K_A)_{Compound} - log\ (\tau/K_A)_{MetEnk}$ (Eq. 2)

For each compound, bias was calculated for Gi2 activation (pathway 1) versus either βarrestin2 recruitment or receptor trafficking in the early endosome compartments (pathway2) (**Table S8**) using the following equation:

$$\Delta\Delta\log(\tau/K_A) = \Delta\log(\tau/K_A)_{pathway1} - \Delta\log(\tau/K_A)_{pathway2} \quad \text{(Eq.3)}$$

Statistically significant bias towards either of the pathways was determined after a one-sample *t* test analysis.

Animals

Male $MOR^{+/+}$ and $MOR^{-/-}$ mice aged 8-16 weeks were bred in-house on a hybrid C57Bl/6J:129SvPas (50:50%) background (Matthes et al, 1996). Male and female $MOR^{+/+}$, $MOR^{Venus/+}$, $MOR^{Venus/Venus}$ mice aged 8-16 weeks were bred in-house on a C57Bl/6N background (Neurophenotyping Center, McGill University/Douglas Hospital Research Institute, Montreal, Canada). $MOR^{Venus/Venus}$ mice were generated at the Institut Clinique de la Souris (Illkirch-Graffenstaden, France). $MOR^{Venus/Venus}$ mice (MOR-Venus mice) expressing the mu opioid receptor fused at its C-terminus to a YFP variant, Venus, were generated by homologous recombination. In these mice, the Venus cDNA was introduced into exon 4 of the *MOR* receptor gene via a targeting construct in which the *MOR* stop codon has been replaced by a Gly-Ser-Ile-Ala-Thr- linker sequence followed by Venus encoding cDNA. A neomycin resistance gene flanked by FRT sites was transfected into embryonic stem (ES) cells (**Figure S2A**). Two independent homologous recombinants were electroporated with an FLP recombinase expressing plasmid to excise the neomycin gene and microinjected into C57Bl/6N blastocysts. F1 heterozygous progenies were obtained from chimeras crossed with C57Bl/6N (Charles River Laboratories, Wilmington, MA, USA) mice. $MOR^{Venus/+}$ mice were intercrossed to generate $MOR^{Venus/Venus}$ mice, which are fertile and develop normally.

Animals were group-housed and maintained on a 12-hour light/dark cycle (lights on at 8:00 AM) at a controlled temperature (22ºC ± 1ºC). Food and water were available *ad libitum* throughout all experiments, unless otherwise stated. All experimental procedures were performed in accordance with the guidelines of the Canadian Council of Animal Care, and all animal procedures were approved by the McGill University/Douglas Hospital Animal Care Committee.

RNA Sample Preparation and Isolation. To collect RNA, brain hemispheres were freshly dissected and immediately frozen on dry ice and stored at -80ºC until use. TRIzol(Invitrogen) reagent was added to the samples directly followed by mechanical dissociation to yield a homogenate. Tissue extraction proceeded according to the manufacture's protocol and Dr. Gentle (Takara, Kusatsu, Japan) was added as a precipitate carrier. Total RNA was re-suspended in RNase-and DNase- free water (ThermoFisher, Waltham, MA, USA). RNA quantity and quality were evaluated spectrophotometrically by NanoDrop ND2000 (ThermoFisher).

RT-qPCR. RT-qPCR was performed as described previously (Erbs et al, 2015) with some modifications. Briefly, 400 ng of RNA was reverse transcribed using the M-MLV Reverse Transcriptase Kit (Invitrogen) according to the manufacturer's instructions. cDNA was diluted 20 times and then subjected to 45 cycles of amplification by using LightCycler 480 SYBR I Green

Master Mix (Roche, Basel, Switzerland) on the LightCycler 480 II Real-Time PCR System (Roche). cDNA samples were loaded in triplicate with 2 µl cDNA and 10 µl final volume. A no-template control (NTC) reaction, with just water, was included to check for non-specific amplification. The housekeeping gene, *B2m,* average was subtracted from the average of the triplicate CT values for each sample. Relative fold changes were calculated by the comparative CT method (2^−ΔΔCT) (Livak & Schmittgen, 2001).

Table of RT-qPCR Primers

Gene	Forward	Reverse
Venus	CACATGAAGCAGCACGACTT	CATTGTGGGCGTTGTAGTTG
mOprm1	CCGAAATGCCAAAATTGTCA	GGACCCCTGCCTGTATTTTGT
mOprd1	GCTCGTCATGTTTGGCATC	AAGTACTTGGCGCTCTGGAA
mBetaActin	GACGGCCAGGTCATCACTAT	CCACCGATCCACACAGAGTA
mB2m	TGGTGCTTGTCTCACTGACC	GTATGTTCGGCTTCCCATTC

[^{35}S] GTPγS binding assay. To evaluate MOR-Venus receptor function in mice, membranes were prepared from rapidly dissected brain hemispheres following mouse cervical dislocation, placed on dry ice and stored at -80ºC until use. For each genotype, 4 male or female mice yielded 4 membrane preparations. Results are expressed as the mean of all preparations.

Membranes were prepared by homogenizing tissue in 0.25M Sucrose (ThermoFisher) with mechanical dissociation for 30 seconds. Centrifugation followed at 2500 rpm, 4ºC for 10 min. Samples were diluted in TMEN (50mM TrisHCl (pH 7.4), 3mM MgCl2, 0.2mM EGTA, 100mM NaCl) and the samples ultracentrifugated (Optimax-XP, Beckman Coultier, Brea, CA, USA) at 40,000 g, 4ºC for 40 minutes with a MLA-55 rotor (Beckman). The membrane pellet was re-suspended in 0.32M sucrose by 10 strokes with a glass tissue grinder. Protein concentration was determined by the Bradford assay (Bio-Rad, Hercules, CA, USA) with a standard curve of BSA (ThermoFisher) and 3 dilutions of each sample. The membrane preparations were diluted to 0.1 mg/ml and stored at -80ºC in aliquots of 500 µl. For each assay, 5 µg of protein was used per well. Samples were incubated with and without ligands, for 1 hour at 25ºC in assay buffer containing 5 mM GDP and 0.1 nM [^{35}S] GTPγS. After filtration (Cell Harvester, Perkin Elmer), bound radioactivity was quantified by a liquid scintillation counter, TopCount (Perkin Elmer). Non-specific binding was determined by binding in the presence of 10 µM GTPγS and basal activity was determined in the absence of agonist. Calculations and sigmoidal dose-response binding curves were done using GraphPad PRISM 6 (GraphPad Software).

Behavioral Tests in MOR-Venus mice. Morphine induced locomotor activity was examined with mice single housed in an empty novel cage located above an infrared floor. Light intensity of the room was set at about 1.5-foot candles. The trajectories of the mice were analyzed and recorder via an automated tracking system equipped with an infrared-sensitive camera (VideoTrack, ViewPoint Behavior Technology, Lyon, France). Behavioral testing started when the animals were placed in the boxes for a 60-minute habituation period. The mice were injected with 40 mg/kg of morphine or saline and activity was assessed for 2 hours. Morphine-induced

analgesia experiments were performed in stable conditions: 23 ± 2°C, 45 ± 5 % humidity, 3.7 ± 0.2-foot candles. The tail immersion test was performed with the mouse restrained in a cylinder exposing only the tail. Mice were injected i.p. with 5 or 10 mg/kg morphine or saline. Briefly, 45 minutes following injection, the tail was immersed in a water bath set at 52°C and tail withdrawal latencies were measured with a cut-off time of 10 seconds. Baseline responses were recorded for 3 days before testing and just before the first injection. In the hot plate test, morphine (5 or 10 mg/kg) or saline was injected i.p. 45 minutes prior to the test. The mouse was placed on a 52°C hot plate and latencies to lick hind limbs were recorded.

Immunohistochemistry. Mice were anesthetized with i.p. injections of 100 µl/100 g of a cocktail containing Ketamine/Xylazine/Acépromazine. Male and female mice were intracardially perfused with 10 ml of 1x PBS pH 7.4 (ThermoFisher) followed by 50 ml of 4% paraformaldehyde or PFA (Cedarlane, Burlington, Canada) in 1x PBS pH 7.4. For whole dissected dorsal root ganglia (DRG), mice were anesthetized as above, heads were severed and DRG were extracted into PBS and then transferred into 4% PFA/1x PBS. Extracted brains or DRG were left for overnight in 10 ml 4% PFA/1x PBS. The next day, tissues were cryoprotected in 30% sucrose (ThermoFisher) 1x PBS pH 7.4 at 4ºC until sunk. Tissues were embedded on dry ice in O.C.T. (Sakura Finetek, Alphen aan den Rijn, Netherlands) and stored at -80ºC until processing. A cryostat (Leica, Wetzlar, Germany) set at -20ºC was used to section tissue. Brain slices were kept free floating in 1x PBS pH 7.4 until staining procedure. DRG were mounted directly from the cryostat onto slides (ThermoFisher) and staining was carried out on the slide. Brain slices of 30 µm were collected in 1x PBS and stored in a 24-well dish (ThermoFisher). Brain and DRG sections were permeabilized in PBS-T (1x PBS pH 7.4, 0.1% Triton X-100) followed by a one-hour incubation with blocking buffer (1x PBS, normal goat serum (NGS; Sigma-Aldrich), 0.2% Triton X-100). For all immunostaining the procedure was as follows, tissue was incubated with primary antibody (for native MORs - Anti-Oprm1 1:1000; Abcam AB134054, Cambridge, United Kingdom and for MOR-Venus - Anti-Venus (GFP) 1:2000, ThermoFisher A111222) diluted in blocking buffer at 4ºC overnight with gentle agitation. The next day, tissue was washed 3 times in PBS-T. Secondary antibody, Alexa Fluor 594 (1:2000, ThermoFisher), was diluted in blocking buffer and incubated with tissue sections for two hours at room temperature with gentle agitation. Tissue were washed 3 times, and in the case of brain sections mounted onto slides. Finally, mounted tissue was sealed with coverslips (ThermoFisher) in Moviol (Sigma-Aldrich) with or without 4',6-diamidino-2-phenylindole (DAPI; ThermoFisher) and left to dry overnight at room temperature with short term storage at 4ºC and long term at -20ºC. For epifluorescence imaging (**Figure 1H** and **Figures S3** and **S4A**), filter cubes were used as indicated (DAPI em.455nm, amplified Venus using Alexa Fluor 488 em.508nm, intrinsic Venus em.527nm, Alexa Fluor 594 Cy3 em. 565nm) and images captured on an Olympus IX73 microscope.

Mapping MOR-Venus. Slide scanner images of coronal brain slices from *MOR*$^{Venus/Venus}$ (n=4), *MOR*$^{Venus/+}$ mice (n=3) and *MOR*$^{+/+}$ mice (n=3) were examined (**Figure 1G** and **Table S1**). MOR-Venus expression was annotated on 44 brain anatomical sub-regions, according to Allen Brain Interactive Atlas Viewer (http://atlas.brain-map.org/). First, all sections were scanned by an Olympus slide scanner VS120 (Olympus Corporation) with a 10x objective and analyzed in

detail using OlyVIA 2.8 software (Olympus Corporation) and VS-Desktop 2.8 (Olympus Corporation), at 5x to 30x magnification. The level of MOR-Venus expression amplified by Anti-Venus antibody (red, was detected using TRITC filter Ex. 535±36 nm, Em. 590±34 nm) was scored by comparing the fluorescence signal between *MOR*$^{+/+}$ corresponding to background level, and *MOR*$^{Venus/+}$ or *MOR*$^{Venus/Venus}$ sections for each brain region of interest. A scale of four levels of fluorescence was used to determine MOR-Venus expression at each region (very low (1), low (2), moderate (3), high (4)). Data for all animals/brain area was pooled to generate a final score. For representative images, we imaged the regional intrinsic MOR-Venus fluorescence (**Figure S4B**) on an Olympus slide scanner VS120 (Olympus Corporation) with a 10x objective. To examine the three patterns of amplified MOR-Venus signal expression (**Figure S4C**): soma, fiber or both cell and fiber illustrated in **Figure 1G**, projections of maximum intensity images were obtained on a confocal microscope. Confocal microscopy analysis of MOR-Venus localization was done using 20x objective lens with 4x zoom to acquire Z-stack images of 0.45 µm steps (anti-Venus ex. 618/ em. 543) on Olympus FV1200 (Olympus Corporation).

Dorsal root ganglia (DRG) neuron culture and immunocytochemistry

To examine agonist-induced MOR-Venus redistribution, DRG neurons were cultured as previously described (Malin et al, 2007). Briefly, male *MOR*$^{+/+}$ or *MOR*$^{Venus/Venus}$ mice aged 8-20 weeks were anesthetized with i.p. injections of 100 µl/100 g of a cocktail containing Ketamine/Xylazine/Acépromazine. Mice were decapitated, and spinal cords were dissected. Using a stereomicroscope (Olympus Corporation) cervical and thoracic DRG were dissected into HBSS Ca/Mg free (ThermoFisher) on ice. In a biosafety tissue culture hood, DRG were minced. The tissue was digested for 30 minutes at 37°C in 2 mg/ml Collagenase/Dispase solution (Millipore, Burlington, MA) in the presence of 200 U/ml DNase (ThermoFisher) to digest tissue. Ganglia were centrifuged briefly at 200 g before removing digestion solution. Ganglia were resuspended in prewarmed culture media containing DMEM/F12 (ThermoFisher), 10% heat inactivated fetal bovine serum (FBS; ThermoFisher) and 1x penicillin-streptomycin (Sigma-Aldrich) and submitted to low-speed centrifugation 200 g. Three repetitions of the washes were done and then ganglia were resuspended in 1 ml of the above media. Ganglia were triturated 10 times with a P1000 pipette, allowed to settle and media was transferred to a new tube in 3 successions. Any remaining undissociated tissue was discarded. DRG suspension was centrifuged for 6 minutes at 1000 g and resuspended in 0.5 ml media. The DRG neuron suspension was applied over a 12.5% and 28% Percoll (GE healthcare, United Kingdom) gradient and centrifuged for 10 minutes at 1300 g. Pelleted DRG neurons were resuspended in 0.25 ml media and centrifuged at 1000 g for 6 minutes and then resuspended in 0.2 ml media and cells diluted 2x in Trypan Blue were counted on hemocytometers (ThermoFisher). DRG neurons were plated onto 12 mm Poly D-Lysine coated coverslips (Neuvitro, Germany) in 24-well plates (ThermoFisher). DRG neurons were cultured at 37°C with 5% CO_2 for 30 minutes to adhere and all media was exchanged for media supplemented with 50 ng/ml nerve growth factor (ThermoFisher).

On day in vitro (DIV) 3, media was removed and washed with DMEM/F12 without supplements. Diluted drugs (concentrations as indicated) or their vehicle (DMSO) were added to

the cells (1 ml per well) at the indicated concentrations in DMEM/F12 without supplements. Cells were returned to incubators for durations indicated and, following drug exposure the plate was placed on ice and the media was removed. Each well was washed 3 times in HBSS followed by incubation with 5 µg/ml WGA-Alexa594 (ThermoFisher) for 10 minutes on ice. The wells were washed 3 more times in HBSS and then fixed in 4% PFA (Electron Microscopy Sciences, Hatfield, PA), 1x PBS (ThermoFisher) for 10 minutes at room temperature. Immediately following, cells were permeabilized in 1x PBS-T (0.1% Triton-X100; ThermoFisher) for 10 minutes. Blocking buffer containing 1x PBS, 3% NGS, 0.2% Triton-X100 was added for 1 hour and the plate was incubated at room temperature with gentle agitation. Primary antibodies anti-Venus (1:2000; Novus Biologicals, NB100-1614, Littleton, CO) or anti-EEA1 (1:500; Cell Signaling Technology, CST3288S, Danver, CT) were diluted in blocking buffer and incubated overnight at 4°C. The following day, the coverslips were washed 3 times in PBS-T for 10 minutes. Secondary antibodies (Alexa Fluor 488; Venus or Alexa Fluor 633; EEA1, 1:2000; ThermoFisher) diluted in blocking buffer were added for 2 hours with gentle agitation at room temperature. Coverslips were finally washed in 1x PBS followed by water before mounting in Moviol (Sigma-Aldrich) onto slides (ThermoFisher). For analysis of MOR-Venus redistribution (**Figure 2E-2G and S9-S10**) and EEA1 co-localization (**Figure 2H-2J and S11**), Z-stack images of 0.45 µm were acquired using an Olympus FV1200 confocal microscope (Olympus Corporation), oil immersion 60x objective lens with 4x zoom (Alexa Fluor 488 Ex. 488/Em. 520, Alexa Fluor 594 Ex. 543/Em. 618, Alexa Fluor 633 Ex. 635/Em. 647).

MOR-Venus IC redistribution assay

For analysis of MOR-Venus DRG neuron confocal images using FIJI (Schindelin et al, 2012),a cell wand plug-in was used to delimit the plasma membrane, on the WGA-Alexa 594 channel, as a region of interest (ROI). Three ROI were made, the original ROI (1.0) a 10% scaled up ROI (1.1) and an inner 20% scaled down ROI (0.8) (see **Figure 2F**). The plasma membrane (PM) was defined as (1.1 - 0.8), the intracellular (IC) portion of the cell as ROI (0.8). To calculate agonist-induced redistribution of MOR-Venus, the signal intensity for IC (0.8) was divided by the total (PM+IC, 1.1). Vehicle treated DRG neurons were included in each set of experiments and the vehicle mean IC was subtracted from each cell. To compare drugs, each IC value was divided by the mean response to Met-Enkephalin and multiplied by 100 (% IC/IC+PM). Data shown are from 3 experiments with 26-52 cells in total, per drug treatment. All data was submitted to a normality test (Shapiro-Wilk) and non-parametric one-way ANOVA was used to examine statistical differences after removing outliers using the ROUT method (Motulsky & Brown, 2006). In each experiment, background fluorescence level was defined as the mean +SEM of the maximum signal intensity detected in $MOR^{+/+}$ DRG neurons. $MOR^{Venus/Venus}$ DRG neuron images (single slice of Z-stack) were analyzed after adjusting the minimum value of intensity to the maximum signal intensity determined by $MOR^{+/+}$ DRG neurons.

MOR-Venus EE co-localization assay

For analysis of MOR-Venus localization at early endosomes (EE) (**Figure 2H-2J and Figure S11**), confocal images were analyzed. A single image from the Z-stack was used with thresholding above background levels for the Venus channel (see MOR-Venus IC redistribution assay). EEA1 channel images were used to identify the location of vesicles and were all equally

adjusted to a signal threshold of 98.5%. The FIJI plug-in, analyze particles, was used to identify and count the number of vesicles stained by anti-EEA1 (**Figure S11C**) and each particle was assigned an ROI to be measured in the Venus channel image (**Figure 2J**). Total Venus particles were divided by total EEA1 particles for each cell to get the ratio of MOR-Venus to EEA1 co-localization. Vehicle treated cells were first quantified and the mean MOR-Venus+/EEA1+ ratio was subtracted from each cell for all treatments. The data was finally normalized to mean Met-Enkephalin induced MOR-Venus+/EEA1+ multiplied by 100. Data shown are from 3 experiments with 26-42 cells in total, per drug treatment. All data was submitted to a normality test (Shapiro-Wilk) and non-parametric one-way ANOVA was carried out after removing outliers using the ROUT method (Motulsky & Brown, 2006).

Statistical Analysis

Statistical significance of the differences was tested using a One-sample *t* test, Mann-Whitney test, one-way or two-way ANOVA with either Dunn's, Dunnett or Bonferroni post hoc adjustment for non-parametric or parametric multiple comparisons, respectively, using GraphPad Prism 6.0 or 7.0 software (GraphPad Software). A value of $P<0.05$ was considered significant.

SUPPLEMENTARY REFERENCES

Black, J. W. & Leff, P. (1983) Operational models of pharmacological agonism. *Proc R Soc Lond B Biol Sci*, 220(1219), 141-62.

Erbs, E., Faget, L., Scherrer, G., Matifas, A., Filliol, D., Vonesch, J. L., Koch, M., Kessler, P., Hentsch, D., Birling, M. C., Koutsourakis, M., Vasseur, L., Veinante, P., Kieffer, B. L. & Massotte, D. (2015) A mu-delta opioid receptor brain atlas reveals neuronal co-occurrence in subcortical networks. *Brain Struct Funct*, 220(2), 677-702.

Kawai, J. & Hayashizaki, Y. (2003) DNA book. *Genome Res*, 13(6B), 1488-95.

Kenakin, T. & Christopoulos, A. (2013) Signalling bias in new drug discovery: detection, quantification and therapeutic impact. *Nat Rev Drug Discov*, 12(3), 205-16.

Leduc, M., Breton, B., Gales, C., Le Gouill, C., Bouvier, M., Chemtob, S. & Heveker, N. (2009) Functional selectivity of natural and synthetic prostaglandin EP4 receptor ligands. *J Pharmacol Exp Ther*, 331(1), 297-307.

Livak, K. J. & Schmittgen, T. D. (2001) Analysis of relative gene expression data using real-time quantitative PCR and the 2(-Delta Delta C(T)) Method. *Methods*, 25(4), 402-8.

Malin, S. A., Davis, B. M. & Molliver, D. C. (2007) Production of dissociated sensory neuron cultures and considerations for their use in studying neuronal function and plasticity. *Nat Protoc*, 2(1), 152-60.

Matthes, H. W., Maldonado, R., Simonin, F., Valverde, O., Slowe, S., Kitchen, I., Befort, K., Dierich, A., Le Meur, M., Dolle, P., Tzavara, E., Hanoune, J., Roques, B. P. & Kieffer, B. L. (1996) Loss of morphine-induced analgesia, reward effect and withdrawal symptoms in mice lacking the mu-opioid-receptor gene. *Nature*, 383(6603), 819-23.

Motulsky, H. J. & Brown, R. E. (2006) Detecting outliers when fitting data with nonlinear regression – a new method based on robust nonlinear regression and the false discovery rate. *BMC Bioinformatics*, 7(1), 123.

Nagi, K. & Pineyro, G. (2016) Practical guide for calculating and representing biased signaling by GPCR ligands: A stepwise approach. *Methods*, 92, 78-86.

Namkung, Y., Le Gouill, C., Lukashova, V., Kobayashi, H., Hogue, M., Khoury, E., Song, M., Bouvier, M. & Laporte, S. A. (2016) Monitoring G protein-coupled receptor and beta-arrestin trafficking in live cells using enhanced bystander BRET. *Nat Commun*, 7, 12178.

Schindelin, J., Arganda-Carreras, I., Frise, E., Kaynig, V., Longair, M., Pietzsch, T., Preibisch, S., Rueden, C., Saalfeld, S., Schmid, B., Tinevez, J. Y., White, D. J., Hartenstein, V., Eliceiri, K., Tomancak, P. & Cardona, A. (2012) Fiji: an open-source platform for biological-image analysis. *Nat Methods*, 9(7), 676-82.

van der Westhuizen, E. T., Breton, B., Christopoulos, A. & Bouvier, M. (2014) Quantification of ligand bias for clinically relevant beta2-adrenergic receptor ligands: implications for drug taxonomy. *Mol Pharmacol*, 85(3), 492-509.